Neuron

Article

A specialized population of hair afferents dedicated to transmitting mechanical itch

Highlights

- TLR5^{Calb1} Aβ-LTMRs innervate vellus-like hairs, forming longitudinal lanceolate endings
- TLR5^{Calb1} Aβ-LTMRs mediate mechanical itch in physiological and pathological states
- Piezo2 in TLR5^{Calb1} Aβ-LTMRs mediates mechanical itch signaling

Authors

Mahar Fatima, Hankyu Lee, Hwayeon Cha, ..., X. Z. Shawn Xu, Yves De Koninck, Bo Duan

Correspondence

bduan@umich.edu

In brief

Fatima et al. identify a specialized sensory pathway in mice in which Piezo2-expressing TLR5^{Calb1} Aβ-LTMRs innervate vellus-like hairs to drive both acute and chronic mechanical itch, revealing a dedicated hair organ for touch-evoked pruritus.

Fatima et al., 2026, Neuron *114*, 1–16
November 11, 2026
https://doi.org/10.1016/j.neuron.2026.05.017

CellPress

Neuron

CellPress

Article

A specialized population of hair afferents dedicated to transmitting mechanical itch

Mahar Fatima,[1,9] Hankyu Lee,[1,9] Hwayeon Cha,[1,9] Chia Chun Hor,[1] Feng Wang,[2] Jingyi Liu,[1] Jonathan Damblon,[2] Wenwen Zhang,[3] Katie Qu,[1] Yumena Nagai,[1] Abbey Dinh,[1] Ziyan Wu,[1] Ranveer Ajimal,[1] Ailin Emily Xiong,[1] Madeleine Chai,[1] Alyssa Asmar,[1] Wei Cai,[3,6] Xiaowei Zhou,[1] Anuraag Balaji,[4] Haili Pan,[1,7] Lorraine Horwitz,[1] Lam C. Tsoi,[4] Hongzhen Hu,[5] X. Z. Shawn Xu,[3,8] Yves De Koninck,[2] and Bo Duan[1,10,*]

[1]Department of Molecular, Cellular, and Developmental Biology, University of Michigan, Ann Arbor, MI 48109, USA
[2]Department of Psychiatry and Neuroscience, CERVO Brain Research Centre, Université Laval, Québec, QC, Canada
[3]Life Sciences Institute, Department of Molecular and Integrative Physiology, University of Michigan, Ann Arbor, MI 48109, USA
[4]Department of Dermatology, Department of Computational Medicine & Bioinformatics, Department of Biostatistics, Mary H. Weiser Food Allergy Center, University of Michigan, Ann Arbor, MI 48109, USA
[5]Department of Dermatology and Neuroscience, The Mark Lebwohl Center for Neuroinflammation and Sensation, Icahn School of Medicine at Mount Sinai, New York, NY, USA
[6]Present address: Institutes of Biomedical Sciences, Inner Mongolia University, Hohhot, Inner Mongolia, China
[7]Present address: Institute of Pain Medicine and Special Environmental Medicine, Co-Innovation Center of Neuroregeneration, Nantong University, Nantong, Jiangsu, China
[8]Present address: Institute of Bio-architecture and Bio-interactions, Shenzhen Medical Academy of Research and Translation (SMART), Shenzhen, Guangdong, China
[9]These authors contributed equally
[10]Lead contact
*Correspondence: bduan@umich.edu
https://doi.org/10.1016/j.neuron.2026.05.017

SUMMARY

Hairs serve as sensory structures that are crucial for perceiving environmental cues through interactions with sensory endings. Depigmented and demedullated atypical hairs exhibit a limited distribution on mammalian skin and have not been extensively studied. In this study, we identify a specific type of hair, termed vellus-like hairs (VLHs), which are enriched in the postauricular region and on the hindpaws of mice. These hairs are innervated by Aβ low-threshold mechanoreceptors (LTMRs) that co-express Toll-like receptor 5 and Calbindin1 (TLR5^{Calb1}). Genetic ablation or silencing of these hair afferents eliminated mechanical itch generated by gentle VLH stroking or indentation under both physiological and pathological conditions. Conversely, optogenetic activation of TLR5^{Calb1} hair afferents evoked itch behaviors. Mechanosensitive Piezo2 channels in TLR5^{Calb1} Aβ-LTMRs function as key mechanotransducers for mechanical itch signaling. Our study sheds light on the previously poorly understood somatosensory physiology of unique hairs, emphasizing the significant role of TLR5^{Calb1} Aβ-LTMRs in itch transmission.

INTRODUCTION

Across the animal kingdom, specialized sensory systems have evolved to navigate complex environments and respond to critical stimuli. Sensory hairs, present across diverse habitats, exhibit a variety of functions, sensitivities, morphologies, specific receptors, and placements on the body.[1] These hairs play a pivotal role in rapid and precise sensory perception, contributing to a wide range of behaviors.[1] In humans, tactile perception is governed by two distinct types of hair: terminal and vellus hairs.[2,3] By contrast, rodents have drawn considerable attention for their pelage hairs, which include guard, awl/auchene, and zig-zag types that are essential for mechanosensation and thermoregulation.[2,4–10] Beyond these well-studied hair types in rodents, certain body regions feature atypical hair variants with unique functions.[11–13] A century ago, a distinct class of "special hairs" was described in mice at defined sites such as the postauricular skin and the area beneath the lower lip.[14] However, the sensory characteristics of these unique hairs, including their associated sensory afferents, have largely been overlooked within sensory biology, and their precise roles remain unknown.

Notably, the anatomical localization of these atypical hairs in exposed or behaviorally sensitive regions suggests that they may support specialized sensory functions beyond canonical touch. One candidate function is itch, a protective sensation that can be elicited by both chemical and mechanical stimuli. Here, we investigated whether these hairs contribute to mechanical itch as a distinct sensory modality. While substantial research has focused on mechanical itch generated by skin indentation,[15–25] hair movement-induced mechanical itch

Please cite this article in press as: Fatima et al., A specialized population of hair afferents dedicated to transmitting mechanical itch, Neuron (2026), https://doi.org/10.1016/j.neuron.2026.05.017

remains relatively unexplored. For instance, the gentle vibration of vellus hair on the chin, in contrast to the forehead, face, or arms, induces intense itching in healthy human subjects.[26] These findings suggest the presence of specialized hair structures and afferents dedicated to this form of mechanical itch. A related clinical phenomenon is trichoknesis, a sensitized itch to hair touch in some chronic itch patients, which is especially relevant to scalp pruritus in inflammatory skin disease or after nerve injury.[27–30] Investigating this less-explored form of mechanical itch has the potential to deepen our understanding of itch sensations and the underlying mechanisms involved.

In this study, we focused on characterizing this class of special hairs in mice, which we termed "vellus-like hairs" (VLHs) due to their resemblance to human vellus hairs. We define their anatomical distribution and sensory innervation and demonstrate their role in mechanical itch evoked by gentle stroking or indentation. We further identify the primary sensory neurons, spinal circuits, and molecular sensors that mediate VLH-dependent acute itch and trichoknesis in chronic conditions. These findings establish a dedicated hair-based pathway for mechanical itch.

RESULTS

Morphological classification and unique sensory innervation of mouse VLHs

Fine and translucent "special hairs" were identified in specific skin regions of mice, including the postauricular area, the transitional zone between glabrous and hairy skin on the lateral hindpaw, and the interdigital space between the hindpaw toes in both 129S1 and C57BL/6J mouse strains (Figures 1A, 1B, and S1). These unique hairs showed reduced or absent pigmentation and contained fewer than 50 or no medulla cells, consistent with previous definitions of atypical hair.[14] Specifically, the postauricular region contained two hair variants: type 1, with elongated imbricate scales, and type 2, with simple coronal scales (Figures 1A and 1C). A third variant, type 3, was found in the transitional zone between glabrous and hairy skin on the lateral hindpaw, the interdigital space between the hindpaw toes, and scattered within the glabrous skin of the sole, displaying a flattened imbricate cuticle (Figures 1B and 1C). These characteristics resemble human vellus hairs, which are characterized by their fine diameter and absence of medulla cells (Figure 1D). Accordingly, we refer to these special hairs as VLHs. By contrast, human scalp hairs contain medulla cells, similar to mouse pelage hairs (Figure 1D).

In rodents, pelage hair follicles typically exhibit a mixed pattern of sensory innervation, including both longitudinal lanceolate and circumferential endings.[4] To investigate the sensory innervation of VLHs, we generated *Advillin*^{Flpo} (*Avil*^{Flpo}) knockin mice (Figures 1E, 1F, and S2A). Crossing with *Rosa26*$^{FSF\text{-}eGFP}$ confirmed targeting 98.4% (3,064/3,114) of dorsal root ganglion (DRG) sensory neurons (Figure 1F). Notably, all three types of VLH follicles across the examined skin regions predominantly exhibited pure longitudinal lanceolate endings. In the postauricular region, 95.6% of type 1 and type 2 VLHs (1,451/1,517) showed exclusive longitudinal lanceolate innervation. Type 3 VLHs showed a similar bias, with 100% of follicles in the sole (14/14) and 96.1% in the interdigital region (124/129) exhibiting this pattern. Pelage hair follicles in the nape overwhelmingly displayed mixed longitudinal and circumferential lanceolate innervation (99.9%, 1,426/1,428) (Figures 1G, 1H, S2B, and S2C).

Identification and characterization of TLR5$^+$ sensory neurons innervating VLHs

To identify the primary sensory neurons innervating VLHs, we performed subcutaneous fluoro-gold (FG) injections into postauricular skin, an area rich in type 1 and type 2 VLHs (Figure 2A). The majority of labeled neurons were NF200$^+$, indicating that VLH afferents predominantly comprise myelinated A low-threshold mechanoreceptors (LTMRs). Minimal overlap was observed with markers of unmyelinated sensory neuron subsets, including tyrosine hydroxylase (TH), calcitonin gene-related peptide (CGRP), isolectin B4 (IB4), somatostatin (Sst), and transient receptor potential melastatin 8 (TRPM8) (Figure S3). Based on prior work linking Toll-like receptor 5-positive (TLR5$^+$) afferents to spinal Ucn3$^+$ itch transmission neurons,[15] we examined *Tlr5* mRNA expression and found that 73.5% (483/657) of FG-labeled neurons expressed *Tlr5* (Figure 2A), consistent with prior reports of endogenous *Tlr5* expression in DRG neurons.[15,31–33] To investigate the functionality of TLR5$^+$ neurons, we generated *Tlr5*$^{P2A\text{-}iCre\text{-}T2A\text{-}EGFP}$ (*Tlr5*^{iCre}) knockin mice (Figures 2B and S4A). Using an intersectional genetic approach,[15] we selectively labeled TLR5-expressing sensory neurons in the DRG by crossing *Tlr5*^{iCre} with *Avil*^{Flpo} and a Cre- and Flpo-dependent tdTomato reporter line (*Rosa26*$^{ds\text{-}tdTomato}$, Ai65), creating *Tlr5*^{iCre};*Avil*^{Flpo};*Rosa26*$^{ds\text{-}tdTomato}$ (TLR5^{Avil}-tdT) mice. 28.3% (920/3,257) of DRG neurons were tdTomato-positive, with 82.2% (1,222/1,486) of *Tlr5* mRNA-expressing neurons showing tdTomato labeling, and 95.8% of tdTomato-positive neurons expressing *Tlr5* mRNA (Figures 2C and S4B). Among these, 62.3% (736/1,181) were NF200$^+$, with smaller fractions expressing CGRP (17.5%, 202/1,152) or IB4 (6.3%, 96/1,535) (Figures 2C and S4B). In VLH-enriched hairy skin, VLH follicles were almost exclusively associated with longitudinal lanceolate endings: 99.2% of type 1/2 follicles in the postauricular region (934/942) and 99.0% of type 3 follicles on the hindpaw (192/194; Figure 2D). In glabrous skin, two predominant patterns were observed: free nerve endings in the epidermis and Meissner corpuscle innervation (Figure S4C).

To assess the mechanosensitivity of TLR5$^+$ neurons innervating VLHs, we performed *in vivo* two-photon Ca^{2+} imaging in the L4-L5 DRGs of *Tlr5*^{iCre};*Rosa26*$^{LSL\text{-}GCaMP6}$ (*Tlr5*^{GCaMP6}) mice, which express GCaMP6s specifically in TLR5$^+$ neurons. We focused on the transitional zone between glabrous and hairy skin on the lateral hindpaw, where type 3 VLHs are located and are readily accessible for controlled mechanical stimulation (Figure 2E). The recordings revealed that all responsive TLR5$^+$ neurons were highly sensitive to gentle stroking of this region and exhibited transient response profiles that rapidly decayed after stimulus onset (Figures 2F and S5). These neurons showed transient responses at both the onset and offset of mechanical indentation across a range of stimulus intensities, with largely non-graded responses to increasing force (Figures 2F, 2I, and S5), consistent with properties reported for rapidly adapting Aβ-LTMRs characterized by *in vivo* Ca^{2+} imaging and electrophysiological recordings.[34,35] At the single-cell level, all recorded TLR5$^+$ neurons that responded to gentle stroking also

Please cite this article in press as: Fatima et al., A specialized population of hair afferents dedicated to transmitting mechanical itch, Neuron (2026), https://doi.org/10.1016/j.neuron.2026.05.017

CellPress

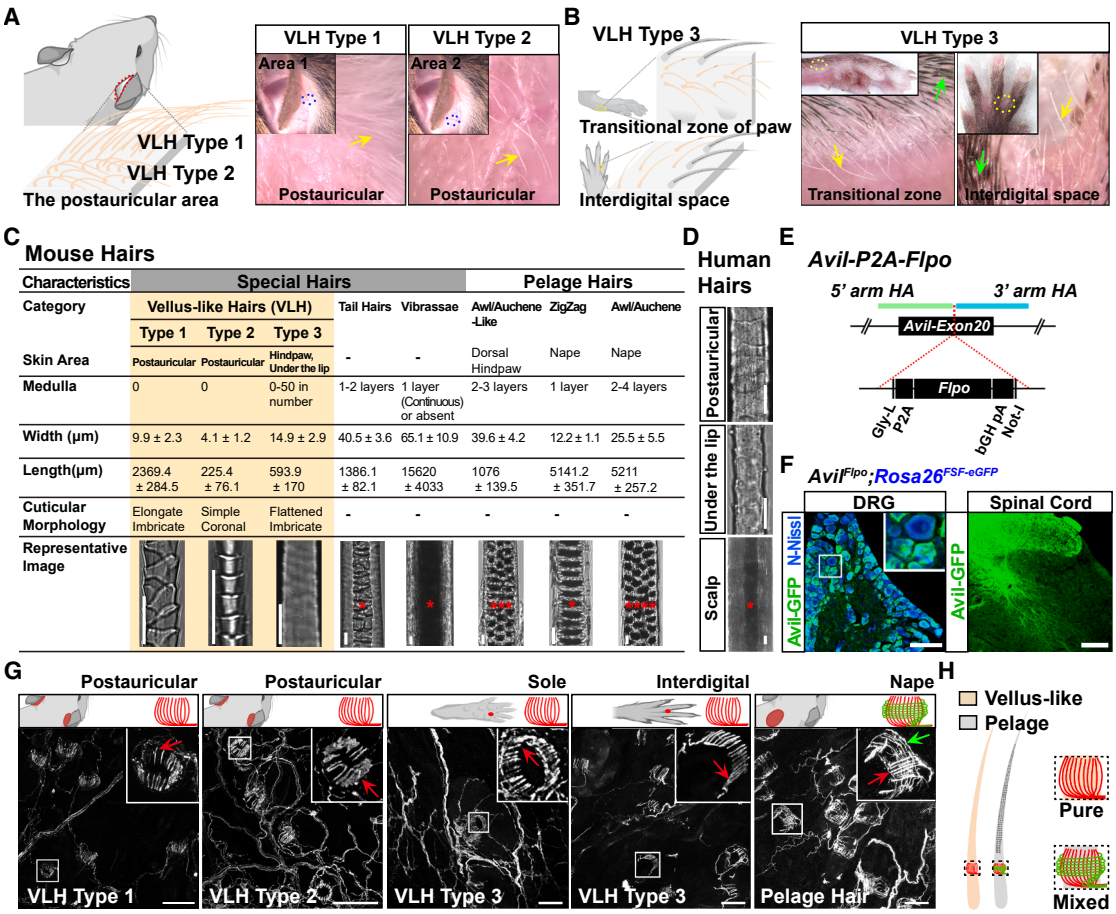

Figure 1. VLHs receive pure longitudinal lanceolate sensory innervation

(A) Vellus-like hairs (VLHs, yellow arrows) in the postauricular area, separated into area 1 and area 2 (dotted blue circles) based on VLH types: types 1 and 2.

(B) Type 3 VLHs (yellow arrows) in the transitional zone between glabrous and hairy hindpaw skin and interdigital space (dotted yellow circles). Green arrows: awl/auchene hair.

(C) Summary of special and terminal hair characteristics in mice. Bottom row shows light microscopic images, and red asterisks indicate medulla layers. ~100–350 hairs from 3–4 mice. Scale bar: 10 μm.

(D) Human vellus hair from ear pinna and lower lip (top, middle). Lower panel: medullated terminal scalp hair. Scale bar: 10 μm.

(E) Schematic of the *Avil*^{Flpo} knockin allele.

(F) Expression of eGFP driven by *Avil*^{Flpo} in DRG neurons and central terminals projecting to the spinal cord in *Avil*^{Flpo};*Rosa26*$^{FSF\text{-}eGFP}$ mice. Neurons visualized by NeuroTrace Nissl (N-Nissl, blue). Scale bar: 100 μm.

(G) Sensory endings of Avil-GFP neurons around VLHs and pelage hairs. Red arrows: longitudinal lanceolate endings. Green arrow: circumferential lanceolate ending. Scale bar: 50 μm.

(H) Organization of sensory endings. VLHs (left) receive pure longitudinal endings, and pelage hairs (right) receive mixed endings.

See also Figures S1 and S2.

responded to indentation stimuli, indicating substantial overlap between these response modalities (Figures 2F and S5), whereas Nav1.8^{+} nociceptors (*SNS*^{Cre}-targeted) exhibited a graded response to indentation stimuli (Figure 2I). These stroking- and indentation-responsive TLR5^{+} neurons were predominantly medium- to large-diameter cells (Figure 2J).

TLR5^{+} sensory neurons transmit mechanical itch

To explore the functional role of TLR5^{+} sensory neurons in mechanical itch, we utilized an intersectional genetic approach by crossing *Tlr5*^{iCre} and *Avil*^{Flpo} with a Cre- and Flpo-dependent *Tau*$^{ds\text{-}DTR}$ line,[36] enabling selective ablation of TLR5^{+} sensory neurons in the DRG. To assess ablation efficiency, we further introduced the Ai65 reporter strain. Histological analysis confirmed that tdTomato expression was restricted to TLR5^{+} sensory neurons, with no labeling of non-neuronal cells in the DRG (Figure 3A). Administration of diphtheria toxin (DT) resulted in efficient and selective ablation of TLR5^{+} sensory neurons (TLR5-Abl) in the DRG, achieving 99.4% efficiency (Figure 3A).

Since VLHs are highly responsive to gentle stroking (Figures 2G and 2H), we developed a behavioral assay to evaluate mechanical itch by gently stroking VLH shafts in the postauricular region with a nylon loop (Figures 3B and S6A). In control mice, this stimulation elicited robust scratching

Please cite this article in press as: Fatima et al., A specialized population of hair afferents dedicated to transmitting mechanical itch, Neuron (2026), https://doi.org/10.1016/j.neuron.2026.05.017

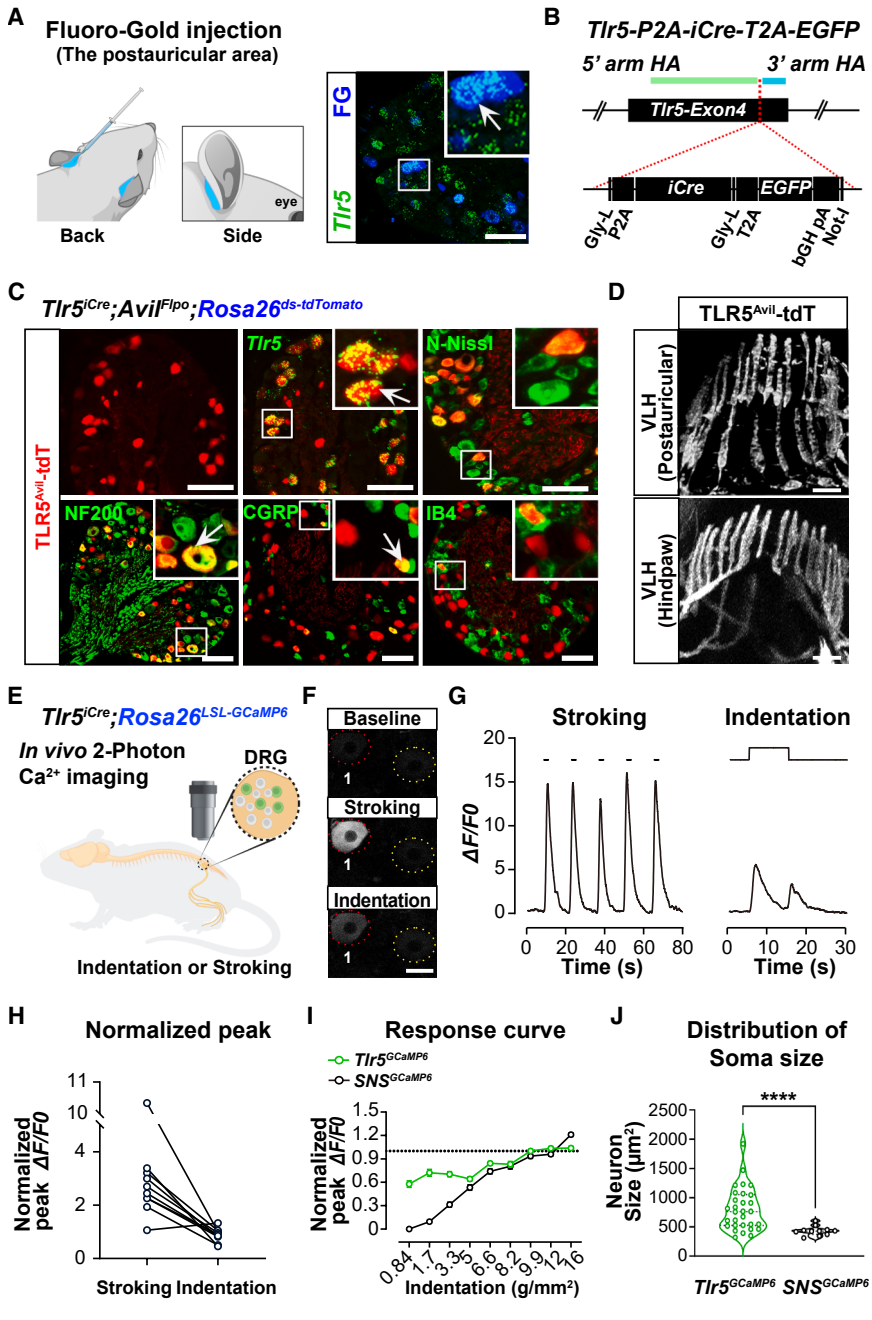

Figure 2. TLR5$^+$ sensory neurons innervate VLH follicles and respond to gentle stroking and indentation stimuli

(A) Schematic demonstrating subcutaneous fluoro-gold (FG) injection in postauricular skin labeling sensory neurons. Right: *Tlr5* mRNA in cervical DRGs. White arrow indicates FG$^+$/*Tlr5*$^+$ neurons. Scale bar: 100 μm.

(B) Schematic of the *Tlr5*^{iCre} knockin allele.

(C) Neurochemical characterization of *Tlr5*^{iCre} targeted cervical DRG neurons (TLR5^{Avil}-tdT). Arrows indicate TLR5^{Avil}-tdT neurons expressing the annotated marker. Scale bars: 100 μm.

(D) Sensory endings of TLR5$^+$ neurons around VLH follicles in postauricular skin and paw transitional zone. Scale bars: 5 μm.

(E) *In vivo* two-photon Ca^{2+} imaging of TLR5$^+$ DRG neurons during stroking or indenting the hindpaw skin.

(F) Ca^{2+} responses (ΔF/F0) during baseline, stroking, and indentation. Red: a neuron responding to both stroking and indentation; yellow: non-responsive. Scale bar: 20 μm.

(G) Ca^{2+} traces showing responses to stroking (left) and indentation (right) of the hindpaw.

(H) Normalized Ca^{2+} responses to stroking or indentation, normalized to 6.6 g/mm^2 indentation. n = 10 from 7 mice.

(I) Normalized Ca^{2+} responses to increasing indentation, normalized to the 9.9 g/mm^2 response of TLR5$^+$ neurons (dashed line), and compared with *SNS*^{Cre} (Nav1.8$^+$) nociceptors. TLR5$^+$, n = 10 from 7 mice; Nav1.8$^+$, n = 12 from 9 mice.

(J) Soma size of stroking-sensitive neurons. TLR5$^+$, n = 30 from 11 mice; Nav1.8$^+$, n = 12 from 9 mice; ****p < 0.0001, two-tailed unpaired Student's t test.

See also Figures S3–S5.

("VLH-itch") that mimics looping vellus hair-induced mechanical itch in humans.[26] In TLR5-Abl mice, scratching was significantly reduced (Figure 3C). To confirm the contribution of TLR5$^+$ neurons, we performed chemogenetic silencing of TLR5$^+$ sensory neurons by expressing the inhibitory DREADD receptor (hM4Di) in *Tlr5*^{iCre};*Avil*^{Flpo};*Rosa26*$^{ds\text{-}hM4Di}$ (TLR5-Sil) mice. Although a previous study reported altered excitability in a subtype of DRG sensory neurons with hM4Di expression,[37] we observed no change in neuronal excitability in TLR5$^+$ sensory neurons with hM4Di expression (Figures S7A–S7I). Administration of clozapine-N-oxide (CNO) in TLR5-Sil mice resulted in a marked reduction in VLH-itch behavioral responses compared with controls (Figure 3D). Previous studies suggest that mechanical itch can also be induced by the gentle indentation of hairy skin.[38,39] Consistent with this, both genetic ablation and chemogenetic silencing of TLR5$^+$ sensory neurons significantly attenuated mechanical indentation-evoked itch, supporting the involvement of the VLH-TLR5$^+$ neuron complex in mechanical itch transmission (Figures 3C and 3D).

By contrast, chemical itch responses to pruritogens, including compound 48/80, chloroquine (CQ), and 5-HT, were unchanged in TLR5-Abl and TLR5-Sil mice (Figure 3E), indicating that TLR5$^+$ neurons are not required for chemical itch. Furthermore, sensorimotor coordination, responsiveness to noxious heat, punctate mechanical pain, noxious mechanical pain, and inflammatory pain remained unaffected by ablation or silencing of TLR5$^+$ sensory neurons (Figures S6B, S6C, S7J, and S7K). Notably, both ablation and acute silencing significantly attenuated mechanical

Please cite this article in press as: Fatima et al., A specialized population of hair afferents dedicated to transmitting mechanical itch, Neuron (2026), https://doi.org/10.1016/j.neuron.2026.05.017

CellPress

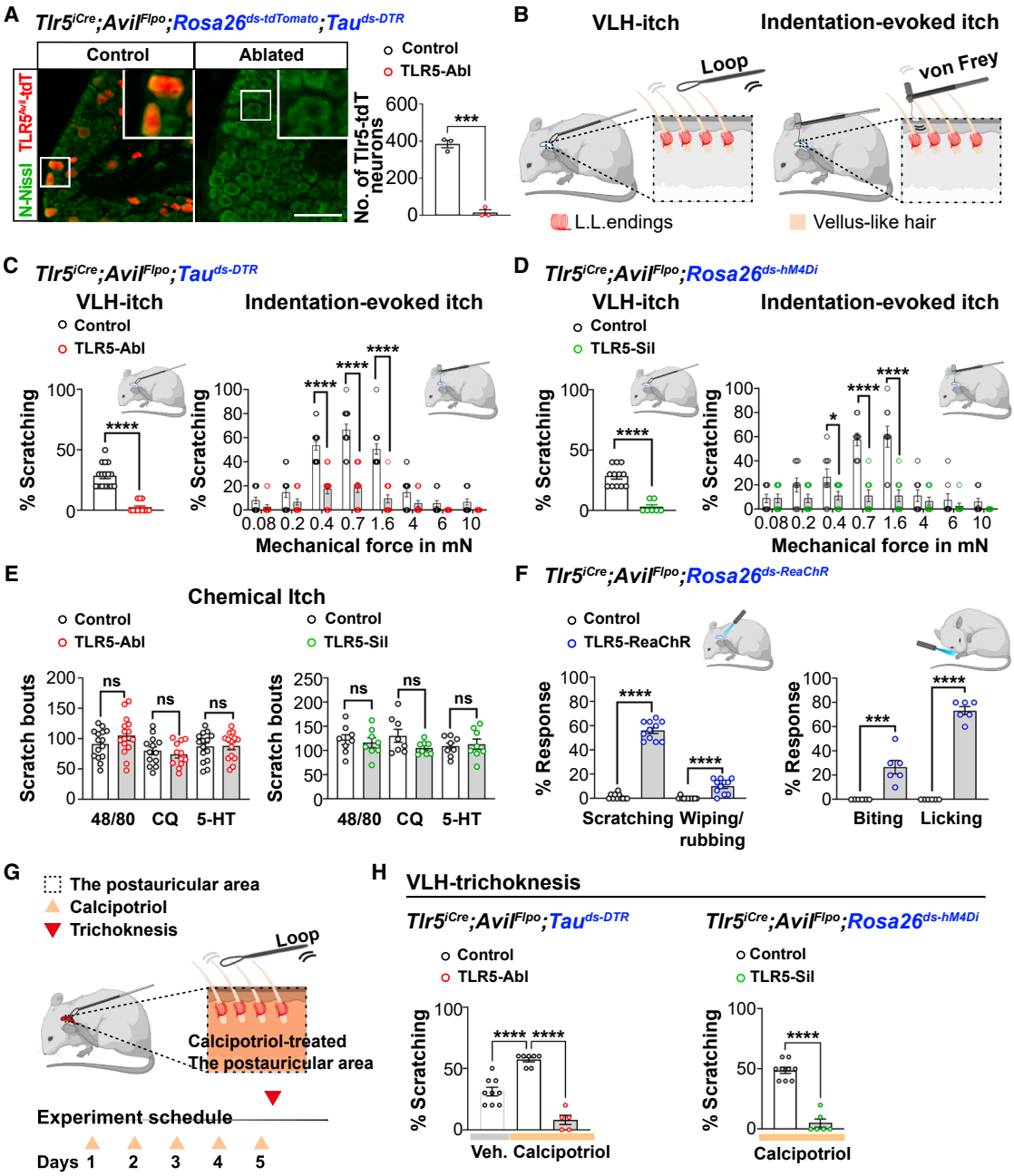

Figure 3. TLR5$^+$ sensory neurons are required for mechanical itch

(A) DRG sections showing TLR5$^+$ neurons in the control (*Tlr5^{iCre};Avil^{Flpo};Rosa26$^{ds\text{-}tdT}$*) and ablated (*Tlr5^{iCre};Avil^{Flpo};Rosa26$^{ds\text{-}tdT}$;Tau$^{ds\text{-}DTR}$*) groups. Scale bar: 100 μm. *n* = 3 DRGs from 3 mice per group.

(B) Postauricular mechanical itch assays: VLH-itch via VLH shaft looping, and indentation-evoked itch via von Frey filament poking.

(C) VLH-itch (left) and indentation-evoked itching (right) in *Tlr5^{iCre};Avil^{Flpo};Tau$^{ds\text{-}DTR}$* (TLR5-Abl) vs. control mice. VLH-itch: control, *n* = 16; TLR5-Abl, *n* = 12. Indentation-evoked itch: *n* = 15 per group.

(D) VLH-itch (left) and indentation-evoked itching (right) in *Tlr5^{iCre};Avil^{Flpo};Rosa26$^{ds\text{-}hM4Di}$* (TLR5-Sil) vs. control mice. VLH-itch: control, *n* = 12; TLR5-Sil, *n* = 7. Indentation-evoked itch: *n* = 9 per group.

(E) Chemical itch responses to compound 48/80, chloroquine (CQ), and 5-HT. For ablation: 48/80: *n* = 15 per group; CQ: control, *n* = 13; TLR5-Abl, *n* = 12; 5-HT: control, *n* = 15, TLR5-Abl: *n* = 14. For silence: *n* = 8 per group.

(F) Optogenetic activation of TLR5$^+$ sensory afferents evokes scratching/wiping (postauricular) or biting/licking (hindpaw). Postauricular: *n* = 11 per group. Dorsolateral hindpaw: *n* = 6 per group.

(G) VLH-trichoknesis induction in a calcipotriol-induced atopic dermatitis model.

(legend continued on next page)

Please cite this article in press as: Fatima et al., A specialized population of hair afferents dedicated to transmitting mechanical itch, Neuron (2026), https://doi.org/10.1016/j.neuron.2026.05.017

allodynia following nerve injury (Figures S6C and S7K), consistent with prior work,[31] suggesting that TLR5^{+} neurons are functionally heterogeneous and might play a role in neuropathic pain.

To test whether TLR5^{+} neuron activation is sufficient to drive itch behavior, we generated TLR5-ReaChR mice by crossing *Tlr5*^{iCre} and *Avil*^{Flpo} with *Rosa26*$^{ds\text{-}ReaChR}$ mice, enabling expression of the red-shifted opsin ReaChR specifically in TLR5^{+} sensory neurons. Optogenetic activation of TLR5^{+} afferents in the postauricular area primarily induced itch-related scratching responses (Figure 3F). Activating TLR5^{+} afferents in the hindpaws of TLR5-ReaChR mice also induced itch-related biting responses (Figure 3F). These findings indicate that activation of TLR5^{+} neurons is sufficient to drive itch behavior, with region-specific motor outputs. Occasional light-induced wiping/rubbing (the postauricular area) and licking (hindpaw) behaviors, often linked to uncomfortable sensations like pain,[38,39] were also observed during pan-TLR5 optogenetic activation (Figure 3F), consistent with functional heterogeneity within the broader TLR5^{+} population and redundancy in nociceptive pathways.

We next evaluated whether TLR5^{+} neurons are required for inflammation-evoked trichoknesis, a sensitized itch response to hair touch in chronic inflammatory itch conditions.[27–30] To test this, we employed a calcipotriol-induced atopic dermatitis model (Figure 3G). In control mice treated with calcipotriol, selective stroking of VLHs significantly increased scratching behavior, which we termed "VLH-trichoknesis" (Figure 3H). Both TLR5-Abl and TLR5-Sil mice showed a marked reduction in VLH-trichoknesis, underscoring the essential role of TLR5^{+} neurons in mediating trichoknesis under chronic itch conditions (Figure 3H). Additionally, calcipotriol-treated TLR5-Abl and TLR5-Sil mice exhibited significantly reduced mechanical alloknesis, a distinct form of mechanical itch sensitization on previously non-pruritic skin in the middle nape region, compared with calcipotriol-treated controls (Figures S6D, S6E, and S7L).

Calb1 co-expression identifies a TLR5^{+} subset required for mechanical itch

Our histological and behavioral analyses of TLR5^{+} sensory neurons revealed a heterogeneous population, which prompted us to investigate a specific subset involved in mechanical itch transmission. To identify this subset, we examined LTMR markers, including Calbindin1 (Calb1), tropomyosin receptor kinase B (TrkB), and vesicular glutamate transporter 3 (VGLUT3). We focused initially on Calb1, which is known to be preferentially expressed in a subset of Aβ-LTMRs.[40] Quantitative analysis revealed that 8.4% (234/2,773) of DRG neurons co-expressed *Tlr5* and *Calb1* mRNA (TLR5^{Calb1}; Figure 4A). The majority of these neurons were myelinated, comprising 7.6% (133/1,750) of DRG neurons, as determined by triple-labeling with NF200 (Figure 4B). We further identified two molecularly distinct subsets within the TLR5^{+} myelinated neuron population: one defined by *Calb1* expression and the other by high-level expression of *Ntrk2* (TrkB^{high}), as detected by *in situ* hybridization.[41,42] Notably, triple-labeling showed minimal overlap among TLR5^{+}, Calb1^{+}, and TrkB^{high} populations, with only 0.2% (5/2,773) of neurons co-expressing all three markers (Figures 4C–4E).

To functionally characterize TLR5^{Calb1} neurons, we performed *in vivo* confocal Ca^{2+} imaging, which enabled simultaneous recording of large neuronal populations in the L4-L5 DRGs of *Tlr5*^{iCre} mice following intrathecal injection of AAV9-CAG-FLEX-GCaMP7f. Whole-mount post hoc DRG hybridization chain reaction (HCR) was subsequently performed to detect *Calb1* mRNA expression across the imaged neuronal populations (Figures 4F and 4G). Our recordings revealed three functionally distinct subpopulations of TLR5^{+} neurons based on their responses to stimulation of VLHs and pelage hairs on both the lateral and dorsal hindpaw skin (Figure S8). The first subset was selectively activated by stroking VLHs on the lateral hindpaw (VLH-selective). The second subset responded exclusively to stimulation of pelage hairs on the dorsal hindpaw (pelage-selective). The third subset responded to both VLHs and adjacent pelage hairs (mixed-responsive) (Figure 4H). *Calb1* mRNA expression was uniformly present in the VLH-selective subset, absent in the pelage hair-selective subset, and detected in a minority of neurons within the dual-responsive population (Figures 4I and 4J).

To confirm that hair shaft displacement is required for activation of TLR5^{+} sensory neurons, we trimmed the VLH shaft and recorded neuronal responses. This trimming significantly attenuated the activity of VLH-selective TLR5^{+} neurons (Figure 4K), indicating that dynamic hair movement is necessary for their activation.

To further investigate the TLR5^{Calb1} subset, we employed *Calb1*^{Cre} mice, which target a heterogeneous population of DRG neurons, including TLR5^{Calb1} neurons (Figures S9A and S9B). Although not exclusive to this subset, *Calb1*^{Cre}-driven strategies allowed us to functionally characterize the broader Calb1^{+} population and delineate the contribution of TLR5^{Calb1} neurons to mechanical itch transmission. AAV-mediated labeling revealed that most Calb1+ endings innervated VLH follicles and formed pure longitudinal lanceolate endings (Figure S9C). *In vivo* confocal Ca^{2+} imaging showed that most Calb1^{+} neurons responded selectively to VLH stimulation, with a minority responding to both VLH and pelage hairs (Figures 4L and 4M).

To assess the function of Calb1^{+} sensory neurons in mechanical itch, we utilized the intersectional ablation strategy to selectively ablate Calb1^{+} DRG neurons (>99% efficiency; Figure S10A). Calb1-ablated (Calb1-Abl) mice showed significant reductions in VLH- and indentation-evoked itch, whereas chemical itch was unaffected (Figures 5A and 5C). Consistently, chemogenetic silencing of Calb1^{+} DRG neurons (Calb1-Sil) markedly reduced VLH- and indentation-evoked itch without altering chemical itch (Figures 5B and 5C). Importantly, there

(H) VLH-trichoknesis in calcipotriol-treated skin. Vehicle-treated control (Veh.), $n = 9$; calcipotriol-treated control, $n = 7$ per group; TLR5-Abl or TLR5-Sil, $n = 6$ per group.

For (A), (C) (VLH-itch), and (D)–(F), two-tailed unpaired Student's t test. For (C) (indentation) and (H), two-way ANOVA with Šídák's multiple comparisons test. $^{*}p < 0.05$, $^{***}p < 0.001$, $^{****}p < 0.0001$; ns, not significant.

See also Figures S6 and S7.

Please cite this article in press as: Fatima et al., A specialized population of hair afferents dedicated to transmitting mechanical itch, Neuron (2026), https://doi.org/10.1016/j.neuron.2026.05.017

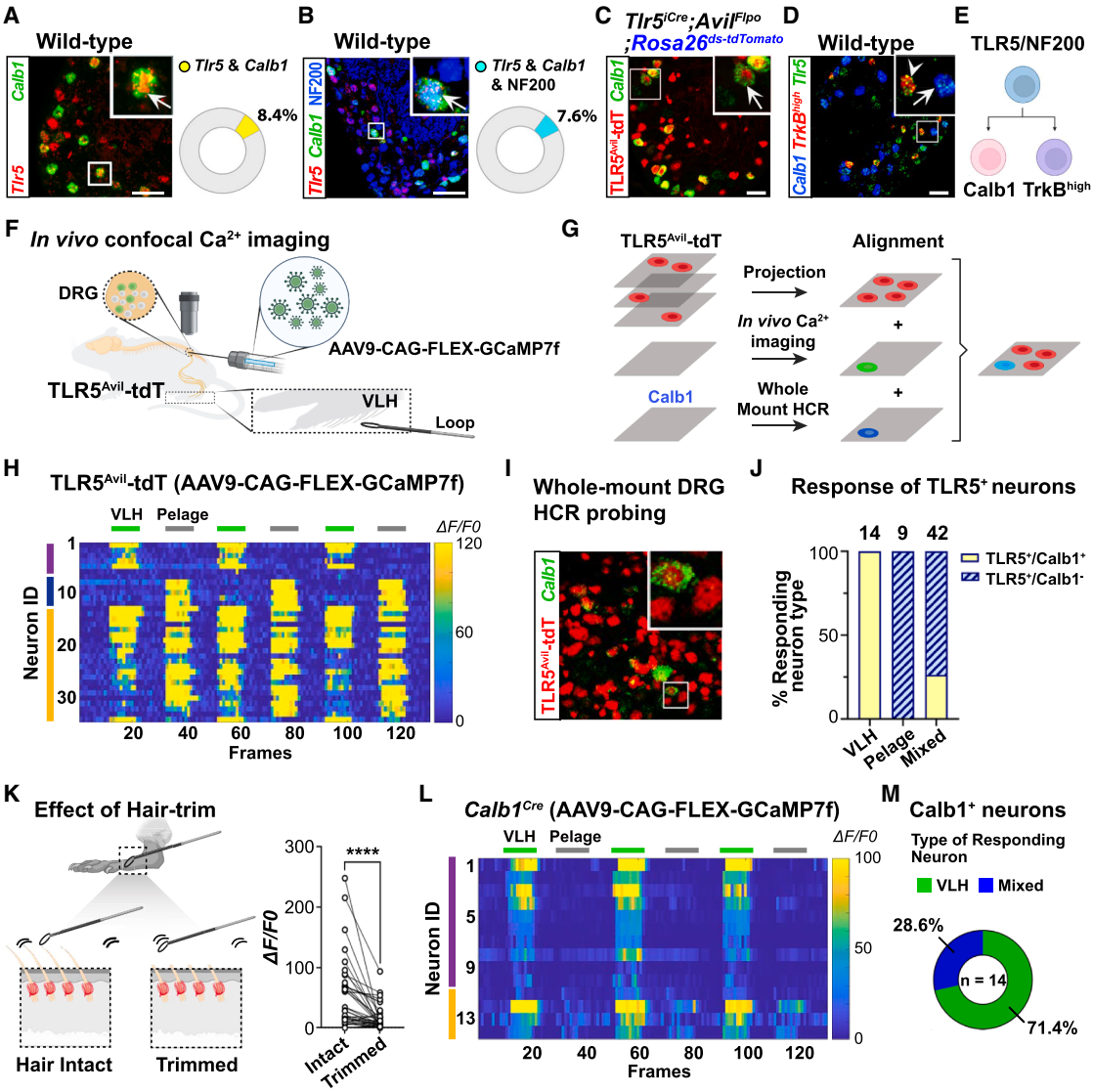

Figure 4. TLR5 and Calb1 co-expression marks a distinct DRG subset selectively activated by VLH stimulation

(A) Co-expression of *Tlr5* and *Calb1* mRNA in DRGs. Arrow indicates a double-positive neuron. n = 19 sections from 3 mice. Scale bar: 100 μm.

(B) Co-expression of *Tlr5* and *Calb1* mRNA in NF200$^+$ neurons. Arrow indicates a triple-positive neuron. n = 13 sections from 3 mice. Scale bar: 100 μm.

(C) *Calb1* mRNA in TLR5^{Avil}-tdT DRGs. Arrow indicates a double-positive neuron. Scale bar: 50 μm.

(D) Co-expression of *Calb1, Ntrk2* (TrkB), and *Tlr5* in DRGs. Arrow indicates a *Calb1*$^+$/*Tlr5*$^+$ neuron. Arrowhead indicates a *TrkB*$^+$/*Tlr5*$^+$ neuron. Scale bar: 50 μm.

(E) Two TLR5$^+$/NF200$^+$ subpopulations: Calb1$^+$ and TrkB^{high}.

(F) *In vivo* confocal Ca^{2+} imaging of TLR5$^+$ DRG neurons in TLR5^{Avil}-tdT mice.

(G) *In vivo* confocal Ca^{2+} imaging followed by z-stack maximum intensity projection of TLR5^{Avil}-tdT and alignment with whole-mount post hoc *Calb1* HCR staining.

(H) Heatmap of Ca^{2+} responses. Neurons are categorized as VLH-selective (purple), pelage-selective (blue), or mixed-responsive (yellow) based on responses to different hair types. n = 34 from 3 mice.

(I) *Calb1* expression in TLR5$^+$ neurons (Z-projection).

(J) Quantification of Calb1$^+$ neurons across functional clusters of TLR5$^+$ neurons. n = 3 mice.

(K) Ca^{2+} responses before and after VLH trimming. n = 35 from 3 mice. ****$p < 0.0001$; two-tailed paired Student's t test.

(L) Heatmap of Ca^{2+} responses in Calb1$^+$ neurons. Neurons are categorized as VLH-selective (purple) or mixed-responsive (yellow). n = 14 from 3 mice.

(M) Functional clusters of Calb1$^+$ DRG neurons. n = 14 from 3 mice.

See also Figures S8 and S9.

Please cite this article in press as: Fatima et al., A specialized population of hair afferents dedicated to transmitting mechanical itch, Neuron (2026), https://doi.org/10.1016/j.neuron.2026.05.017

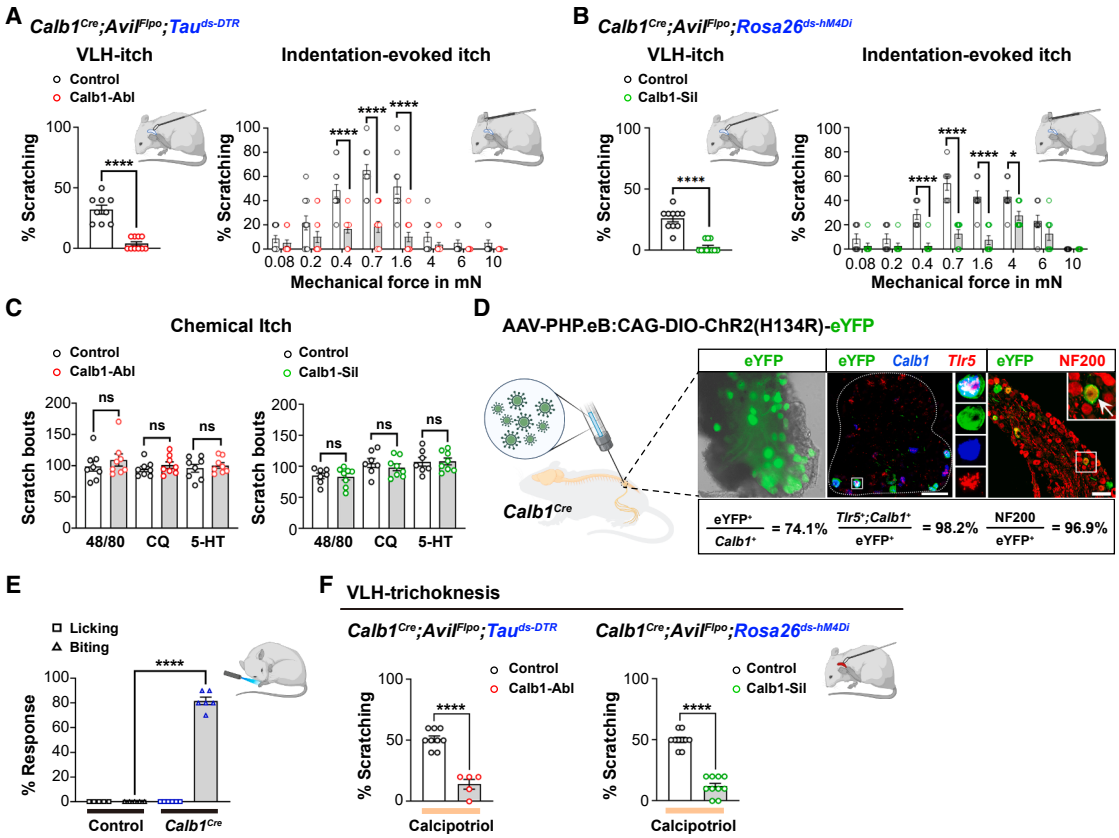

Figure 5. Calb1^{+} sensory neurons are required for mechanical itch

(A) VLH-itch (left) and indentation-evoked itching (right) in *Calb1^{Cre};Avil^{Flpo};Tau$^{ds\text{-}DTR}$* (Calb1-Abl) vs. control mice. VLH-itch: control, $n = 9$; Calb1-Abl, $n = 10$. Indentation-evoked itch: $n = 12$ per group.

(B) VLH-itch (left) and indentation-evoked itching (right) in *Calb1^{Cre};Avil^{Flpo};Rosa26$^{ds\text{-}hM4Di}$* (Calb1-Sil) vs. control mice. VLH-itch: control, $n = 10$; Calb1-Sil, $n = 12$. Indentation-evoked itch: control, $n = 7$; Calb1-Sil, $n = 8$.

(C) Chemical itch responses to compound 48/80, chloroquine (CQ), and 5-HT. For ablation: $n = 8$ per group. For silence: control, $n = 7$ per group; Calb1-Sil, $n = 8$ per group.

(D) AAV.PHP.eB.CAG-DIO-ChR2(H134R)-eYFP injection into lumbar DRG of *Calb1^{Cre}* mice. Left: whole-mount DRG showing eYFP expression. Middle: YFP-labeled Calb1^{+} neurons probed for *Calb1* and *Tlr5* mRNA. Scale bar: 50 μm. Right: YFP-labeled Calb1^{+} neurons probed for NF200. Scale bar: 100 μm. Arrow indicates an NF200^{+} neuron. $n = 4$ mice.

(E) Responses to optogenetic activation of Calb1^{+} DRG neuron terminals in the dorsolateral hindpaw. Control, $n = 5$; Calb1^{Cre}, $n = 6$.

(F) VLH-trichoknesis in the atopic dermatitis model. For ablation: control, $n = 9$; Calb1-Abl, $n = 5$. For silence: $n = 10$ per group.

For (A), (B) (VLH-itch), (C), (E), and (F), two-tailed unpaired Student's *t* test. For (A) and (B) (indentation), two-way ANOVA with Šídák's multiple comparisons test. $^{*}p < 0.05$, $^{****}p < 0.0001$; ns, not significant.

See also Figures S10–S12.

were no differences in sensorimotor coordination, noxious heat responses, inflammatory pain, or chronic pain sensitivity between Calb1-Abl or Calb1-Sil mice and controls (Figures S10B, S10C, S10E, and S10F).

Region-specific silencing using retrograde AAV-DIO-hM4Di(Gi)-mCherry targeted postauricular-projecting Calb1+ neurons enriched for TLR5^{Calb1} (84.6%, 22/26) (Figure S11A). hM4Di expression did not alter the intrinsic excitability of infected TLR5^{Calb1} neurons (Figure S11B–S11I). CNO administration reduced both VLH-itch and indentation-evoked itch (Figures S11J and S11K), consistent with genetic ablation and silencing.

To test sufficiency, AAV-PHP.eB-DIO-ChR2-eYFP was injected into L4-L5 DRGs of *Calb1^{Cre}* mice to enable optogenetic stimulation of Calb1^{+} afferents in the hindpaw. eYFP labeling covered 74.1% of Calb1^{+} neurons, and eYFP^{+} neurons were highly enriched for *Tlr5^{+}/Calb1^{+}* (98.2%) and NF200^{+} (96.9%) (Figure 5D). Light stimulation of Calb1^{+} terminals evoked robust biting without licking (Figure 5E), indicating that activation of this TLR5^{Calb1} population is sufficient to drive itch behavior.

In the calcipotriol-induced atopic dermatitis model, ablation or silencing of Calb1^{+} neurons significantly attenuated VLH-trichoknesis (Figure 5F), further supporting the essential role of TLR5^{Calb1} neurons in sensitized mechanical itch responses.

In comparison, selective ablation of the other two LTMR subtypes that form longitudinal lanceolate endings had no effect on itch and other sensory modalities (Figure S12). Specifically, ablating TrkB^{high} neurons, which innervate both pelage hairs[40–42]

Please cite this article in press as: Fatima et al., A specialized population of hair afferents dedicated to transmitting mechanical itch, Neuron (2026), https://doi.org/10.1016/j.neuron.2026.05.017

and VLH, and VGLUT3^{+} sensory neurons, which innervate pelage hairs,[43,44] did not affect VLH-itch or indentation-evoked itch. Notably, TrkB^{high} neurons represent a distinct subset of the TLR5^{+} population and mediate mechanical allodynia after nerve injury, highlighting functional divergence within TLR5^{+} subtypes.

TLR5^{Calb1} afferents form longitudinal lanceolate endings on VLH follicles and mediate mechanical itch

Our preceding analyses using *Tlr5^{iCre}* and *Calb1^{Cre}* mice implicated a TLR5^{Calb1} subpopulation in the DRG in the detection of VLH-mediated mechanical itch. However, both lines label molecularly heterogeneous neuronal populations, limiting the subtype-specific resolution. To genetically isolate this intersectional population, we generated *Calb1^{Flpo}* mice (Figure S13A). We first validated Flpo recombinase activity in *Calb1^{Flpo}* mice using *Rosa26$^{FSF\text{-}eGFP}$*. RNAscope *in situ* hybridization confirmed high concordance between eGFP and *Calb1* expression: 98.7% (384/389) of eGFP^{+} neurons co-expressed *Calb1*, and 94.8% (384/405) of Calb1^{+} neurons expressed eGFP (Figure 6A), thereby supporting the specificity and efficiency of the *Calb1^{Flpo}* allele.

To genetically define TLR5^{Calb1} neurons, we crossed *Tlr5^{iCre}* and *Calb1^{Flpo}* mice with Ai65 (TLR5^{Calb1}-tdT). In the DRG, 95.2% (518/544) of tdTomato^{+} neurons co-expressed *Tlr5* and *Calb1*, and 96.8% (518/535) of *Tlr5^{+}/Calb1^{+}* neurons were labeled with tdTomato (Figure 6B). In comparison, no TLR5^{Calb1} double-positive neurons were detected in the spinal cord or brain (Figure S13B). Screening across the entire DRG axis (C1-S1) revealed that TLR5^{Calb1} neurons are broadly distributed, with relative enrichment at cervical and lumbar levels corresponding to VLH-rich skin regions (Figures S13C and S13D). In C1-C2 DRGs, TLR5^{Calb1} neurons accounted for approximately 7.1% of total DRG neurons (452/6,372) (Figure S13D), providing a quantitative estimate of their abundance at this VLH-enriched level.

We next examined the terminal morphology of TLR5^{Calb1} neurons in the skin. TdTomato^{+} afferents formed characteristic longitudinal lanceolate endings on VLH follicles, with high specificity in the postauricular (94.3%; 383/406) and hindpaw (88.3%; 143/162) regions. These terminals were rarely observed around pelage follicles in the nape (4.6%; 18/395), indicating that TLR5^{Calb1} neurons preferentially innervate VLHs. In contrast to hairy skin, analysis of the glabrous skin revealed that none of the Meissner's corpuscles examined (0%; 0/298) showed tdTomato labeling, and no tdTomato^{+} profiles were detected in the epidermis, demonstrating that TLR5^{Calb1} neurons neither innervate Meissner's corpuscles nor form free nerve endings in the epidermis (Figure 6D).

To further define their molecular identity, we performed co-labeling with markers of hair follicle-innervating LTMR subtypes. Ret, TrkB/*Ntrk2*, and TH each define distinct subclasses of longitudinal lanceolate afferents that innervate hair follicles.[4] Among TLR5^{Calb1} neurons, 98.9% (369/373) were NF200^{+}, 35.2% (148/421) co-expressed Ret, and TrkB^{high} expression was rare (1.7%; 6/322) (Figures 6C and S13E). TH and CGRP were absent (Figure S13E), excluding C-LTMRs and Aδ circumferential high-threshold mechanoreceptors.[34,45] These data support a myelinated longitudinal lanceolate LTMR identity that is molecularly distinct from canonical hair-associated subtypes.

To determine their conduction properties, we performed compound action potential recordings following selective ablation of TLR5^{Calb1} neurons using the DTR-based intersectional genetic approach. Ablation efficiency was first confirmed, as TLR5^{Calb1}-tdT neurons were eliminated in the DRG (Figure S14A). Ablation selectively reduced the Aβ component of the compound action potential without affecting Aδ or C-fiber responses (Figure S14B and S14C), indicating that TLR5^{Calb1} neurons contribute to the Aβ fiber population and are consistent with an Aβ-LTMR identity.

Next, we assessed the functional role of TLR5^{Calb1} neurons in mechanical itch. Selective ablation of TLR5^{Calb1} neurons led to significant reductions in both VLH-itch and indentation-evoked itch behaviors (Figure 6E), with chemical itch, light touch, thermal sensitivity, acute mechanical pain, and chronic pain remaining intact (Figures 6G, S15A, and S15B). We further examined whether mechanical stimulation of non-VLH regions could evoke itch under our experimental conditions. Mechanical stimulation of glabrous hindpaw skin did not reliably induce scratching in control mice: neither hair-independent looping nor focal indentation elicited measurable itch-like responses, and no differences were observed in TLR5^{Calb1}-Abl mice (Figure S15C). These results demonstrate that TLR5^{Calb1} neurons are selectively required for VLH-dependent mechanical itch but are dispensable for chemical itch and pain-related behaviors.

To test whether activation of TLR5^{Calb1} neurons is sufficient to elicit itch-related behaviors, we performed optogenetic activation of cutaneous TLR5^{Calb1} terminals in *Tlr5^{iCre};Calb1^{Flpo};Rosa26$^{ds\text{-}ReaChR}$* mice. Blue light stimulation applied to the postauricular region elicited robust scratching (Figure 6F; Video S1), whereas stimulation of the hindpaw induced stereotyped biting responses (Figure 6F; Video S2). However, light stimulation of the nape did not produce scratching or wiping/rubbing responses (Figure S15D; Video S1). These findings demonstrate that selective activation of TLR5^{Calb1} afferents in VLHs is sufficient to evoke regionally specific mechanical itch behaviors, without eliciting pain-associated responses such as wiping or licking. Consistent with this, local application of the TLR5 ligand flagellin to the postauricular region induced scratching that was abolished in TLR5^{Calb1}-Abl mice, whereas flagellin application to the nape failed to evoke itch responses (Figure S15E). Because co-application of flagellin and the membrane-impermeant sodium channel blocker QX-314 selectively silences TLR5^{+} neurons,[15,31] we next tested whether this manipulation suppresses optogenetically evoked scratching. Co-application of flagellin and QX-314 to the postauricular region nearly completely abolished light-evoked scratching (Figure S15F), further supporting that region-specific activation of TLR5^{Calb1} afferents is required to drive mechanical itch behaviors.

In the calcipotriol-induced chronic itch model, selective ablation of TLR5^{Calb1} neurons significantly reduced VLH-trichoknesis (Figure 6H), mechanical alloknesis (Figure S15G), and eventually spontaneous scratching behaviors (Figure 6H). These findings demonstrate that the TLR5^{Calb1} subset is required for the expression of mechanical itch sensitization and ongoing scratching in this chronic itch paradigm.

To determine whether a functionally analogous population exists in humans, we examined cultured human dorsal root ganglion

Please cite this article in press as: Fatima et al., A specialized population of hair afferents dedicated to transmitting mechanical itch, Neuron (2026), https://doi.org/10.1016/j.neuron.2026.05.017

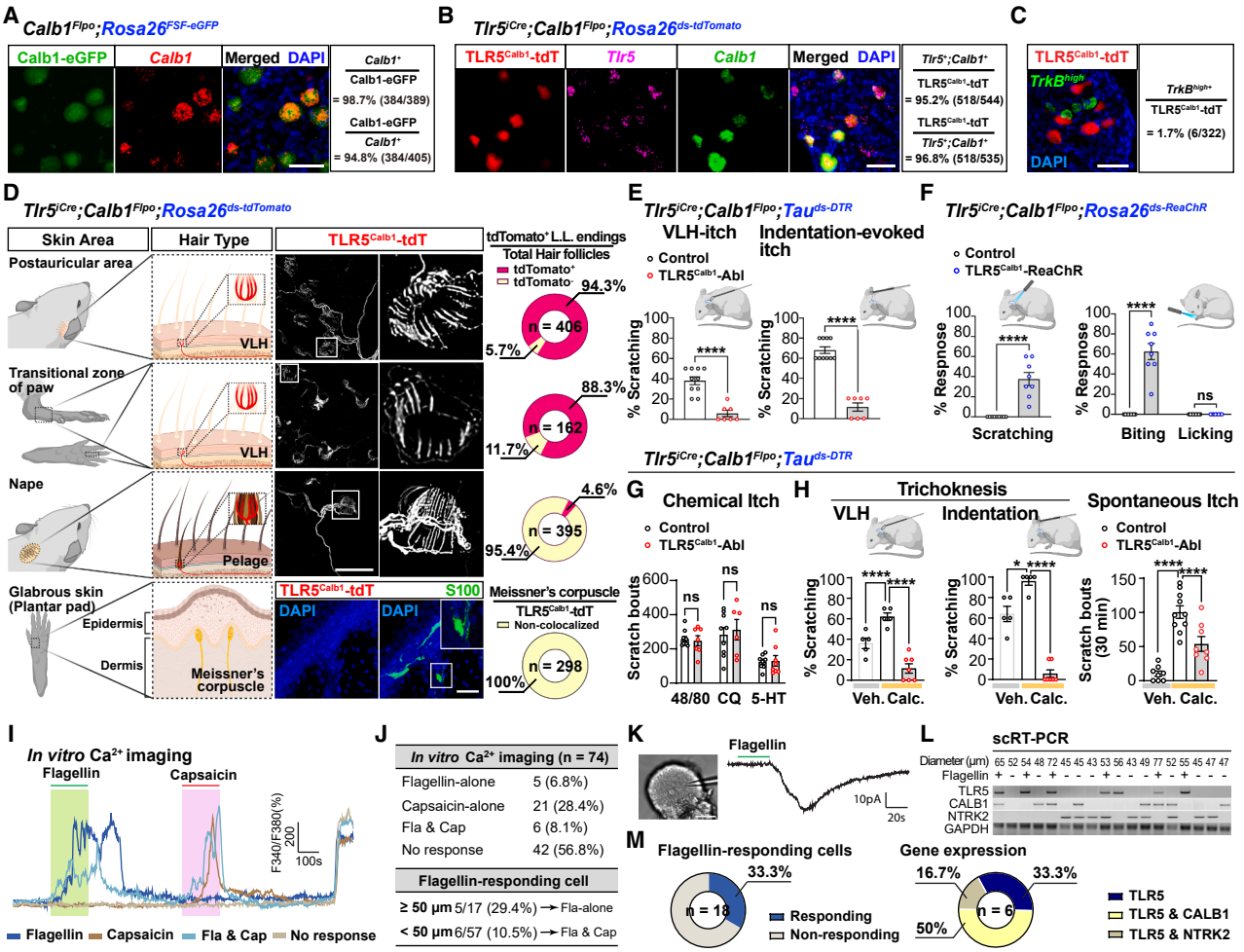

Figure 6. TLR5^{Calb1} sensory neurons form longitudinal lanceolate endings on VLH follicles and mediate mechanical itch

(A) Validation of Flpo activity in *Calb1^{Flpo};Rosa26$^{FSF\text{-}eGFP}$* mice. $n = 31$ sections from 3 mice. Scale bar: 50 μm.

(B) Characterization of TLR5^{Calb1} neurons in *Tlr5^{iCre};Calb1^{Flpo};Rosa26$^{ds\text{-}tdTomato}$* (TLR5^{Calb1}-tdT) mice. $n = 29$ sections from 3 mice. Scale bar: 50 μm.

(C) Co-localization of TLR5^{Calb1}-tdT neurons with TrkB^{high} DRG neurons. $n = 23$ sections from 3 mice. Scale bar: 50 μm.

(D) Cutaneous innervation by TLR5^{Calb1}-tdT neurons. L.L.: longitudinal lanceolate endings. $n = 20$–30 sections from 3–5 mice. Scale bars: 100 μm, 25 μm (bottom).

(E) VLH-itch and indentation-evoked itch in *Tlr5^{iCre};Calb1^{Flpo};Tau$^{ds\text{-}DTR}$* (TLR5^{Calb1}-Abl) vs. control mice. Control, $n = 10$; TLR5^{Calb1}-Abl, $n = 7$.

(F) Responses to optogenetic activation of TLR5^{Calb1} DRG neuron terminals in the postauricular skin (left) and lateral hindpaw (right) of *Tlr5^{iCre};Calb1^{Flpo};Rosa26$^{ds\text{-}ReaChR}$* (TLR5^{Calb1}-ReaChR) mice. Control, $n = 9$; TLR5^{Calb1}-ReaChR, $n = 8$.

(G) Chemical itch responses to compound 48/80, chloroquine (CQ), and 5-HT. Control, $n = 9$–10 per group; TLR5^{Calb1}-Abl, $n = 6$–7 per group.

(H) Trichoknesis and persistent spontaneous scratching in the atopic dermatitis model. Left: VLH- and indentation-evoked trichoknesis. Vehicle-treated (Veh.) and calcipotriol-treated (Calc.) control, $n = 5$ per group; Calc. TLR5^{Calb1}-Abl, $n = 6$. Right: spontaneous scratching quantified over 30 min after 7 days of topical calcipotriol treatment. Veh, $n = 8$; calc. control, $n = 10$; Calc. TLR5^{Calb1}-Abl, $n = 8$.

(I) *In vitro* Ca^{2+} imaging of human DRG neurons showing responses to flagellin (5 nM, green) and capsaicin (1 μM, red).

(J) Quantification of Ca^{2+} responses. $n = 74$.

(K) Flagellin (5 nM, green bar)-evoked inward current in a large-diameter human DRG neuron. Scale bar: 25 μm.

(L) Single-cell RT-PCR analysis of recorded human DRG neurons following recording.

(M) Summary of electrophysiological and gene expression results. $n = 18$.

For (E)–(G), two-tailed unpaired Student's *t* test. For (H), two-way ANOVA with Šídák's multiple comparisons test. $^{*}p < 0.05$, $^{****}p < 0.0001$; ns, not significant. See also Figures S13–S15.

neurons. *In vitro* Ca^{2+} imaging revealed that 5 of 74 neurons (6.8%) responded selectively to flagellin alone, and all were large-diameter neurons (≥50 μm),[46,47] consistent with a low-threshold mechanosensory phenotype. Conversely, flagellin and capsaicin dual-responsive neurons were restricted to small-diameter cells (< 30 μm) (Figures 6I and 6J). Whole-cell patch-clamp recordings followed by single-cell RT-PCR identified flagellin-responsive neurons expressing TLR5 alone or co-expressing TLR5 and CALB1 (Figures 6K–6M), revealing a molecularly defined human DRG population with features analogous to mouse TLR5^{Calb1} Aβ-LTMRs.

Please cite this article in press as: Fatima et al., A specialized population of hair afferents dedicated to transmitting mechanical itch, Neuron (2026), https://doi.org/10.1016/j.neuron.2026.05.017

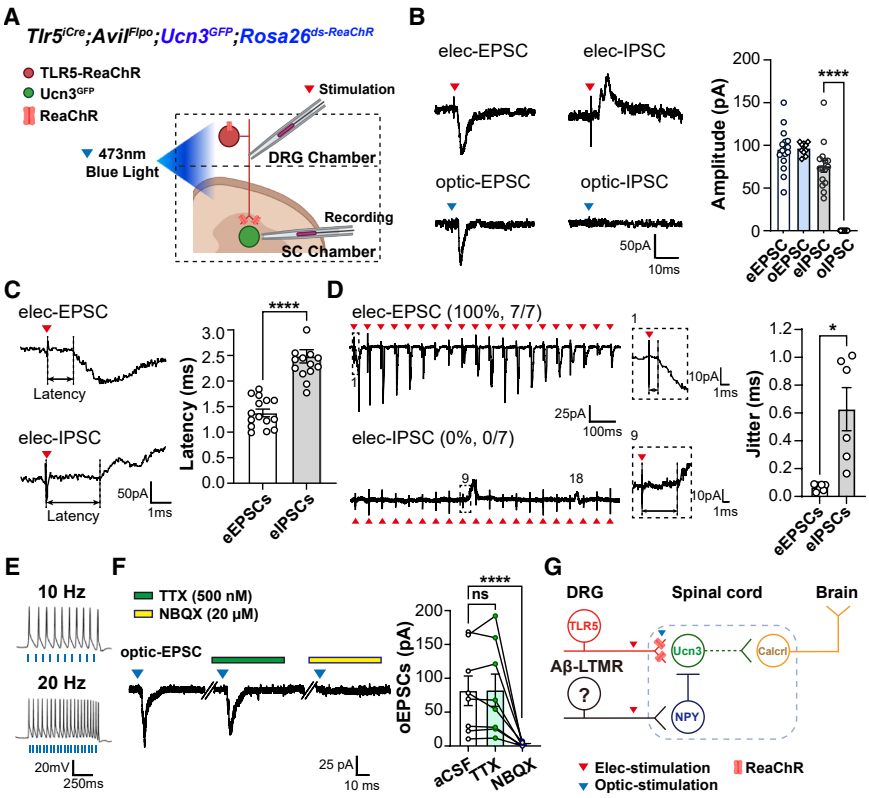

Figure 7. TLR5$^+$ Aβ-LTMRs form monosynaptic excitatory synapses onto spinal Ucn3$^+$ itch transmission neurons

(A) Recording configuration in a two-chamber DRG-spinal cord slice preparation in *Tlr5^{iCre};Avil^{Flpo};Ucn3^{GFP};Rosa26$^{ds\text{-}ReaChR}$* mice. Red arrowhead: electrical stimulation of Aβ fibers.

(B) Synaptic responses in Ucn3$^+$ neurons following electrical stimulation of Aβ fibers (elec-EPSC, elec-IPSC) or optogenetic activation of TLR5$^+$ afferents (optic-EPSC, optic-IPSC). $n = 15$ from 6 mice.

(C) Onset latency analysis of electrically evoked responses. Traces from (B) are expanded to illustrate latency measurements. $n = 15$ from 6 mice.

(D) Synaptic reliability and temporal jitter. Left: responses to trains of 20 electrical stimuli (red arrowheads) in Ucn3$^+$ neurons. Insets show expanded views. Right: temporal jitter of EPSCs ($n = 7$) and IPSCs ($n = 6$) from 3 mice.

(E) Optogenetic stimulation of TLR5$^+$ afferents (473 nm, 1 ms pulses; cyan bars) and action potential firing in Ucn3$^+$ neurons at 10 and 20 Hz. $n = 15$ from 6 mice.

(F) Light-evoked EPSCs in Ucn3$^+$ neurons in the presence of TTX (500 nM) and NBQX (20 μM). $n = 8$ from 6 mice.

(G) Schematic of the experimental configuration and VLH mechanical itch circuit.

For (B) and (F), two-way ANOVA with Tukey's multiple comparisons test. For (C) and (D), two-tailed unpaired Student's *t* test. *$p < 0.05$, ****$p < 0.0001$.

Together, these findings establish TLR5^{Calb1} neurons as a distinct Aβ-LTMR subtype that selectively innervates VLHs and mediates mechanical itch in mice, with a molecularly analogous population present in human DRG.

TLR5$^+$ sensory neurons provide monosynaptic excitatory inputs to spinal itch transmission neurons

Although our previous study implicated TLR5$^+$ primary afferents in transmitting indentation-evoked mechanical itch via pharmacological silencing and anatomical mapping,[15] direct genetic and synaptic evidence linking these neurons to identified spinal targets remained lacking. To address this, we employed intersectional genetic tools in combination with electrophysiological approaches to assess the functional connectivity between TLR5$^+$ DRG neurons and Ucn3$^+$ spinal neurons. Using *Tlr5^{iCre};Avil^{Flpo};Ucn3^{GFP};Rosa26$^{ds\text{-}ReaChR}$* mice, we recorded synaptic responses in Ucn3$^+$ neurons evoked by either electrical stimulation of dorsal root Aβ fibers or optogenetic activation of TLR5$^+$ afferents (Figure 7A).

Non-selective electrical stimulation of Aβ fibers evoked both excitatory postsynaptic currents (EPSCs) and inhibitory postsynaptic currents (IPSCs) in Ucn3^{GFP} neurons (Figure 7B), indicating that these neurons receive both direct excitation and polysynaptic inhibition from the broader Aβ afferent population. By contrast, selective optogenetic activation of TLR5$^+$ terminals elicited EPSCs but no detectable IPSCs (Figure 7B), suggesting that activation of TLR5$^+$ afferents does not recruit inhibitory interneurons onto Ucn3$^+$ neurons.

To distinguish mono- vs. polysynaptic components under electrical stimulation, we analyzed synaptic onset latency and temporal reliability. Electrically evoked EPSCs exhibited significantly shorter onset latencies than IPSCs (Figure 7C). Trains of 20 consecutive electrical stimuli reliably evoked EPSCs in all recorded Ucn3$^+$ neurons (7/7), with responses observed on every trial, whereas IPSCs were inconsistently evoked across sweeps and frequently failed during stimulus trains (Figure 7D), indicating reduced synaptic reliability. Temporal jitter, calculated as the standard deviation of onset latency across trials, was extremely low for EPSCs (66.2 ± 8.8 μs), consistent with monosynaptic transmission. IPSCs exhibited significantly higher jitter (627.8 ± 154.9 μs) (Figure 7D), indicative of polysynaptic signaling.

To directly test whether TLR5$^+$ afferents form monosynaptic excitatory connections onto Ucn3$^+$ neurons, we examined synaptic responses elicited by selective light activation. Increasing light stimulation frequency proportionally increased action potential firing in Ucn3$^+$ neurons without failure (Figure 7E). Light-evoked EPSCs persisted in tetrodotoxin (TTX) and were abolished by 2,3-dioxo-6-nitro-1,2,3,4-tetrahydrobenzo[f]quinoxaline-7-sulfonamide (NBQX), an antagonist of α-amino-3-hydroxy-5-methyl-4-isoxazolepropionic acid (AMPA) receptor (Figure 7F), establishing direct glutamatergic transmission from TLR5$^+$ afferents. Collectively, these findings demonstrate that TLR5$^+$ DRG neurons form functional monosynaptic excitatory synapses onto spinal Ucn3$^+$ itch transmission neurons, defining a peripheral-spinal microcircuit for VLH-mediated mechanical itch (Figure 7G).

Please cite this article in press as: Fatima et al., A specialized population of hair afferents dedicated to transmitting mechanical itch, Neuron (2026), https://doi.org/10.1016/j.neuron.2026.05.017

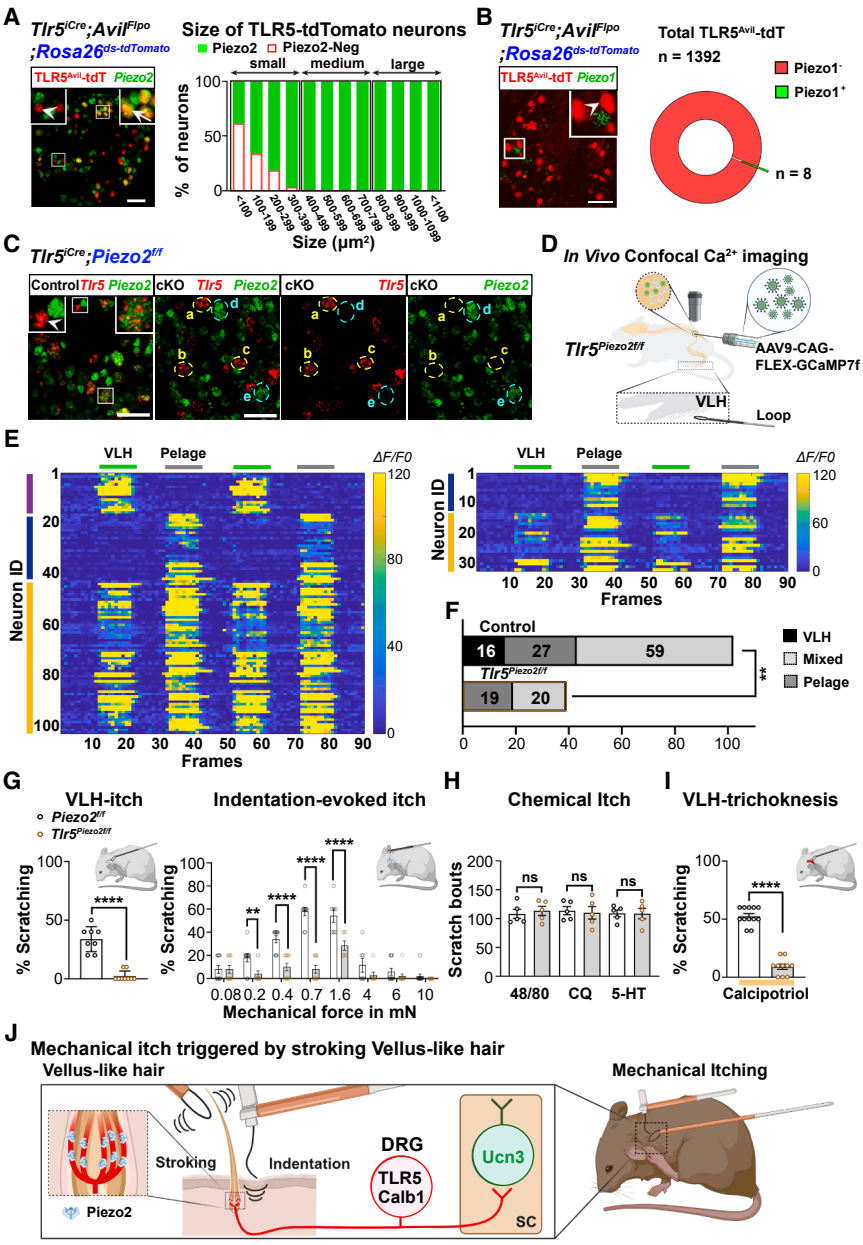

Figure 8. Piezo2 channels in TLR5$^+$ Aβ-LTMRs mediate mechanical itch

(A) *Piezo2* mRNA expression in DRGs of TLR5^{Avil}-tdT mice. Arrow indicates a *Piezo2*$^+$ TLR5^{Avil}-tdT neuron. Arrowhead indicates a *Piezo2*$^-$ neuron. Right: size distribution of *Piezo2*$^+$ TLR5^{Avil}-tdT neurons. Scale bar: 100 μm.

(B) *Piezo1* mRNA expression in DRGs of TLR5^{Avil}-tdT mice. Arrowhead indicates a *Piezo1*$^+$ TLR5^{Avil}-tdT neuron. Scale bar: 100 μm.

(C) Co-expression of *Tlr5* and *Piezo2* mRNA in DRGs of control and *Tlr5*^{iCre};*Piezo2*$^{flox/flox}$ (*Tlr5*$^{Piezo2f/f}$) mice. arrowhead: *Piezo2*$^-$/TLR5$^+$ neuron. Yellow circles: *Tlr5*$^+$ neurons lacking *Piezo2*. Cyan circles: *Piezo2*$^+$ neurons lacking *Tlr5*. Scale bars: 100 μm.

(D) *In vivo* confocal Ca^{2+} imaging of DRGs of *Tlr5*$^{Piezo2f/f}$ mice.

(E) Heatmaps of Ca^{2+} responses in control (*Tlr5*^{iCre} + AAV9-CAG-FLEX-GCaMP7f, left) and *Tlr5*$^{Piezo2f/f}$ cKO (*Tlr5*^{iCre};*Piezo2*$^{f/f}$ + AAV9-CAG-FLEX-GCaMP7f, right) neurons, categorized as VLH-selective (purple), pelage-selective (blue), or mixed-responsive (yellow). Control, *n* = 102 neurons from 4 mice; *Tlr5*$^{Piezo2f/f}$ cKO, 32 neurons from 4 mice.

(F) Quantification of *in vivo* confocal Ca^{2+} imaging data across groups.

(G) VLH-itch (left) and indentation-evoked itch (right) in *Tlr5*$^{Piezo2f/f}$ vs. control mice. Control, *n* = 8; *Tlr5*$^{Piezo2f/f}$ cKO, *n* = 9.

(H) Chemical itch responses to compound 48/80, chloroquine (CQ), and 5-HT. *n* = 5 per group.

(I) VLH-trichoknesis in *Tlr5*$^{Piezo2f/f}$ vs. control mice. Control, *n* = 12; *Tlr5*$^{Piezo2f/f}$, *n* = 10.

(J) Summary model of VLH-mediated mechanical itch: Piezo2-expressing TLR5^{Calb1} Aβ-LTMRs innervate VLHs and transmit touch signals to spinal Ucn3$^+$ neurons to drive mechanical itch.

For (F), the chi-square test, $\chi^2 = 10.61$, df = 2. For (G) (VLH-itch), (H), and (I), two-tailed unpaired Student's *t* test. For (G) (indentation), two-way ANOVA with Šídák's multiple comparisons test. $^{**}p < 0.01$, $^{****}p < 0.0001$; ns, not significant.

See also Figure S16.

Piezo2 channels are molecular sensors that transmit mechanical itch

The ability of somatosensory neurons to detect mechanical stimuli relies on mechanotransduction proteins that convert physical forces into electrical signals through conformational changes. Among these, Piezo2 is a key mechanosensitive ion channel expressed in LTMRs and is essential for innocuous touch perception.[48] Previous studies have shown that conditional knockout (cKO) of *Piezo2* in sensory neurons leads to a significant decrease in rapidly adapting mechanocurrents.[48] Based on this, we investigated whether Piezo2 contributes to the molecular transduction of VLH-itch mediated by Aβ-LTMRs. We first examined Piezo2 expression in TLR5$^+$ sensory neurons in the DRG and found that *Piezo2* mRNA was selectively expressed in medium- to large-diameter TLR5$^+$ neurons (>400 μm^2), whereas *Piezo1* mRNA was rarely detected (Figures 8A and 8B). To elucidate the specific role of Piezo2 channels in TLR5$^+$ sensory neurons, we generated a cKO strain (*Tlr5*$^{Piezo2f/f}$) by crossing *Tlr5*^{iCre} with *Piezo2*$^{f/f}$ and confirmed the deletion of *Piezo2* (Figure 8C).

To test whether VLH stroking requires Piezo2-mediated activation of TLR5$^+$ DRG neurons, we performed intrathecal injection of AAV9-CAG-DIO-GCaMP7f followed by *in vivo* confocal Ca^{2+} imaging in both *Tlr5*^{iCre} control mice and *Tlr5*$^{Piezo2f/f}$ mice (Figure 8D). To classify response types, VLH-selective neurons were defined as those responding exclusively to VLH stimulation, mixed neurons as those responding to both VLH and adjacent pelage hairs, and pelage-selective neurons as those responding only to pelage hair stimulation. In control mice, all three response types were observed. In TLR5$^+$ neurons lacking *Piezo2*,

Please cite this article in press as: Fatima et al., A specialized population of hair afferents dedicated to transmitting mechanical itch, Neuron (2026), https://doi.org/10.1016/j.neuron.2026.05.017

VLH-selective responses were completely abolished, whereas mixed responses were markedly reduced (Figures 8E and 8F).

Behaviorally, both VLH-itch and indentation-evoked itch were significantly diminished in *Tlr5*$^{Piezo2f/f}$ mice (Figure 8G). These behavioral impairments closely resembled those observed following genetic ablation of TLR5^{Calb1} neurons, underscoring the indispensable role of Piezo2 channels in mediating mechanical itch. No deficits were observed in motor coordination, thermal nociception, acute mechanical pain, and chemical itch (Figures 8H and S16A). *Tlr5*$^{Piezo2f/f}$ mice also displayed a modest reduction in nerve injury-induced mechanical hypersensitivity (Figure S16B), suggesting a potential contribution of the TLR5^{+}/Calb1^{-} subpopulation. Notably, calcipotriol-induced trichoknesis was nearly abolished, and mechanical alloknesis was markedly reduced in *Tlr5*$^{Piezo2f/f}$ mice (Figures 8I and S16C), emphasizing the essential role of Piezo2-mediated signaling in the development of chronic mechanical itch sensitization.

In summary, our findings establish Piezo2 channels as the main mechanotransducer in TLR5^{Calb1} DRG neurons that innervate VLH follicles and mediate mechanical itch. This molecular specialization allows these afferents to specifically encode low-threshold mechanical stimuli and transmit itch-related information to second-order spinal Ucn3^{+} neurons. The anatomical targeting of VLH follicles and their functional role in mechanical itch behaviors highlight the central importance of TLR5^{Calb1} neurons and Piezo2 channels in both acute and chronic itch states. These findings emphasize a distinct sensory pathway for mechanical itch and lay the groundwork for targeted treatments for chronic itch disorders (Figure 8J).

DISCUSSION

Hair serves multiple functions as a specialized appendage of the skin, including thermoregulation, physical protection, and tactile reception.[2] Medulla- and pigment-deficient vellus hairs in humans are mechanosensitive,[49] potentially sensing itch,[26] and detecting ectoparasites.[50] Vellus hairs are found near mucosal openings (e.g., ear, nose, and mouth), where they may help detect external threats such as parasites or pathogens. In mice, we observed depigmented, medulla-free VLHs in the postauricular region, as well as in the interdigital spaces and along the transition between glabrous and hairy skin of the lateral hindpaw. Although these hindpaw VLHs do not mirror the distribution of human vellus hairs, their positioning in exposed, touch-sensitive areas suggests an evolutionarily conserved sensory surveillance function. The mechanosensitivity of VLHs and vellus hairs may suggest a role in dual protective systems for mechanical and chemical itch in humans and animals.[50–53] Mechanical itch, triggered by VLH deflection, promotes scratching or brushing behaviors to remove irritants. In parallel, chemical itch, activated by pruritic compounds, reinforces the detection of threats even without direct contact. Together, these mechanisms provide a coordinated protective system across exposed body regions.

Although nociception and pain also serve as critical alarm systems, our results show that TLR5^{Calb1} neurons do not contribute to acute and chronic pain. Consistent with this, forceful pulling of VLH hairs primarily elicited escape-like responses (rapid movement away or brief head shaking) rather than classical nocifensive wiping, and these responses were preserved in TLR5^{Calb1}-Abl mice (Figures S15H and S15I). These findings suggest that VLH-associated TLR5^{Calb1} afferents are specialized for mechanical itch rather than nociceptive signaling.

Our molecular characterization experiments revealed that TLR5^{+} sensory neurons are a heterogeneous population, including Aβ, Aδ, and C subtypes. Although recent single-cell RNA sequencing studies report that *Ntrk2* transcripts are expressed in approximately one-fourth of DRG neurons, with a large fraction overlapping with *Calb1* transcripts,[54,55] these percentages are substantially higher than estimates from more traditional methods. *In situ* hybridization and genetic reporter strategies, including *TrkB*^{CreER}, consistently identify less than 10% of DRG neurons as expressing high levels of TrkB.[41,42] The TrkB^{high} population targeted by *TrkB*^{CreER} likely corresponds to the TrkB^{+}/Calb1^{-} subset of TLR5^{+} Aδ-LTMRs that innervate both pelage hairs and VLHs, thereby encompassing a broader pool of mixed and pelage hair-sensitive responders. *TrkB*^{CreER} and *Calb1*^{Cre} label largely non-overlapping subsets of A-LTMRs that innervate the same hair follicles with intermarginal longitudinal lanceolate endings.[40] Prior work suggests that TrkB^{+} A-LTMRs encode directional hair deflection,[41] whereas TLR5^{Calb1} neurons mediate VLH-mediated mechanical itch.

Various LTMR subclasses contribute to different aspects of mechanosensation.[4,34] Piezo1 mediates indentation-evoked mechanical itch in pelage skin.[17] Interestingly, TLR5^{Calb1} sensory neurons do not express *Piezo1*, whereas Piezo2 is present and mediates VLH-itch. We propose that mechanical itch involves two distinct sensory neuron populations: Piezo1-expressing Sst^{+}/Nppb^{+} C-pruriceptors, which respond to chemicals like histamine and IL-31 as well as indentation,[17] and Piezo2-expressing TLR5^{Calb1} Aβ-LTMRs, which appear dedicated to transmitting VLH-itch and indentation-evoked mechanical itch. Piezo1 is enriched in Sst^{+}/Nppb^{+} C-high-threshold mechanoreceptors (C-HTMRs) that form free nerve endings and respond to high-threshold mechanical stimuli.[56] By contrast, VLH-evoked itch engages myelinated TLR5^{Calb1} neurons that respond to low-threshold hair movement, form NF200^{+} longitudinal lanceolate endings around VLHs, and are required for VLH-evoked itch behaviors.

Mechanical itch sensitization is a common symptom in many skin disorders.[57,58] The connection between TLR5^{Calb1} Aβ-LTMRs and VLHs, as well as the essential role of TLR5^{Calb1} neurons in transmitting VLH-trichoknesis, suggests a link to chronic hair-related itch conditions like scalp pruritus, though the mechanisms remain unclear. We also observed that TLR5^{Calb1} Aβ-LTMRs contribute to mechanical alloknesis following cutaneous inflammation of the ear or acute pruriceptor activation (Figure S15J), as indicated by indentation-evoked itch responses at typically non-pruritic sites such as the nape. Notably, optogenetic stimulation of the nape in naive TLR5^{Calb1}-ReaChR mice failed to elicit itch behaviors, suggesting that TLR5^{Calb1} afferents innervating pelage hairs, though sparse, are likely silent under physiological conditions. Under inflammatory or pruritogen-sensitized states, however, these afferents may become sensitized and be required for transmission of mechanical itch or alloknesis.

Taken together, our study provides insights into the somatosensory physiology of specialized hairs, emphasizing the critical role of TLR5^{Calb1} Aβ-LTMRs in transmitting itch triggered by hair touch. These specialized hairs and their associated nerve terminals are crucial for regulating trichoknesis in chronic itch, underscoring their importance in abnormal sensory processing.

RESOURCE AVAILABILITY

Lead contact

Further information and requests for resources and reagents should be directed to the lead contact, Dr. Bo Duan (bduan@umich.edu).

Materials availability

Transgenic animals generated in this study are available from the lead contact upon request and completion of a material transfer agreement.

Data and code availability

- This study did not generate any unique datasets requiring deposition in a public repository.
- This paper does not report original code.
- Any additional information required to reanalyze the data reported in this work is available from the lead contact upon request.

ACKNOWLEDGMENTS

We acknowledge Dr. Thom Saunders and the Transgenic Animal Model Core of the University of Michigan for the preparation of *Avil*^{Flpo} and *Tlr5*^{iCre} mouse strains. The *Calb1*^{Flpo} mouse strain was created in collaboration with Cyagen. We thank Dr. Martyn Goulding for *Tau*$^{ds\text{-}DTR}$ knockin mice, Dr. David Ginty for *TrkB*^{CreER} knockin mice, Dr. Bradford Lowell for *VGLUT3*^{Cre} knockin mice, Dr. Rohini Kuner for *SNS*^{Cre} transgenic mice, Dr. Ardem Patapoutian for *Piezo2*$^{f/f}$ mice, and Dr. Susan Dymecki for *Rosa26*$^{ds\text{-}hM4Di}$ and *Rosa26*$^{FSF\text{-}eGFP}$ knockin mice. Funding: This study was supported by B.D.'s start-up grant at the University of Michigan and, in part, by NIH grants (B.D., X.Z.S.X., H.H., and L.C.T.). Y.D.K. was supported by a Canadian Institutes of Health Research Foundation grant and a Canada Research Chair in Chronic Pain and Related Brain Disorders. H.L. was supported by an NIH T32 training grant.

AUTHOR CONTRIBUTIONS

Conceptualization, B.D.; methodology, M.F., H.L., H.C., C.C.H., J.L., J.D., F.W., W.Z., K.Q., Y.N., R.A., A.E.X., M.C., A.A., W.C., X.Z., H.P., L.H., H.H., X.Z.S.X., Y.D.K., and B.D.; investigation, M.F., H.L., H.C., C.C.H., J.L., J.D., F.W., W.Z., A.E.X., K.Q., Y.N., R.A., X.Z., M.C., and A.A.; visualization, M.F., H.L., H.C., J.L., J.D., F.W., W.Z., C.C.H., A.E.X., K.Q., Y.N., A.D., Z.W., R.A., X.Z., M.C., A.A., and A.B.; writing – original draft, M.F., H.L., F.W., and B.D.; writing – review & editing, M.F., H.L., H.C., C.C.H., Y.D.K., and B.D.; funding acquisition, B.D., Y.D.K., X.Z.S.X., H.H., L.C.T., and H.L.

DECLARATION OF INTERESTS

The authors declare no competing interests.

STAR★METHODS

Detailed methods are provided in the online version of this paper and include the following:

SUPPLEMENTAL INFORMATION

Supplemental information can be found online at https://doi.org/10.1016/j.neuron.2026.05.017.

Received: October 14, 2025
Revised: March 3, 2026
Accepted: May 14, 2026

REFERENCES

1. Jablonski, N.G. (2004). The evolution of human skin and skin color. Annu. Rev. Anthropol. *33*, 585–623. https://doi.org/10.1146/annurev.anthro.33.070203.143955.
2. Schneider, M.R., Schmidt-Ullrich, R., and Paus, R. (2009). The hair follicle as a dynamic miniorgan. Curr. Biol. *19*, R132–R142. https://doi.org/10.1016/j.cub.2008.12.005.
3. Vogt, A., Hadam, S., Heiderhoff, M., Audring, H., Lademann, J., Sterry, W., and Blume-Peytavi, U. (2007). Morphometry of human terminal and vellus hair follicles. Exp. Dermatol. *16*, 946–950. https://doi.org/10.1111/j.1600-0625.2007.00602.x.
4. Handler, A., and Ginty, D.D. (2021). The mechanosensory neurons of touch and their mechanisms of activation. Nat. Rev. Neurosci. *22*, 521–537. https://doi.org/10.1038/s41583-021-00489-x.
5. Lechner, S.G., and Lewin, G.R. (2013). Hairy sensation. Physiology *28*, 142–150. https://doi.org/10.1152/physiol.00059.2012.
6. Li, L., Rutlin, M., Abraira, V.E., Cassidy, C., Kus, L., Gong, S., Jankowski, M.P., Luo, W., Heintz, N., Koerber, H.R., et al. (2011). The functional organization of cutaneous low-threshold mechanosensory neurons. Cell *147*, 1615–1627. https://doi.org/10.1016/j.cell.2011.11.027.
7. Rice, F.L., and Albrecht, P.J. (2008). Cutaneous mechanisms of tactile perception: morphological and chemical organization of the innervation

to the skin. In The Senses: a Comprehensive Reference, *6*, A.I. Basbaum, A. Kaneko, G.M. Shepherd, and G. Westheimer, eds. (Academic Press), pp. 1–31. https://doi.org/10.1016/B978-012370880-9.00340-6.

8. Romanovsky, A.A. (2014). Skin temperature: its role in thermoregulation. Acta Physiol. *210*, 498–507. https://doi.org/10.1111/apha.12231.
9. Lumpkin, E.A., Marshall, K.L., and Nelson, A.M. (2010). The cell biology of touch. J. Cell Biol. *191*, 237–248. https://doi.org/10.1083/jcb.201006074.
10. Johnson, K.O., and Hsiao, S.S. (1992). Neural mechanisms of tactual form and texture perception. Annu. Rev. Neurosci. *15*, 227–250. https://doi.org/10.1146/annurev.ne.15.030192.001303.
11. Ahl, A.S. (1986). The role of vibrissae in behavior: a status review. Vet. Res. Commun. *10*, 245–268. https://doi.org/10.1007/BF02213989.
12. Hickman, G.C. (1979). The mammalian tail: a review of functions. Mamm. Rev. *9*, 143–157. https://doi.org/10.1111/j.1365-2907.1979.tb00252.x.
13. Cohn, J.F., Xiao, J., Moriyama, T., Ambadar, Z., and Kanade, T. (2003). Automatic recognition of eye blinking in spontaneously occurring behavior. Behav. Res. Methods Instrum. Comput. *35*, 420–428. https://doi.org/10.3758/bf03195519.
14. Dry, F.W. (1926). The coat of the mouse (Mus musculus). J. Genet. *16*, 287–340. https://doi.org/10.1007/BF02983004.
15. Pan, H., Fatima, M., Li, A., Lee, H., Cai, W., Horwitz, L., Hor, C.C., Zaher, N., Cin, M., Slade, H., et al. (2019). Identification of a Spinal Circuit for Mechanical and Persistent Spontaneous Itch. Neuron *103*, 1135–1149.e6. https://doi.org/10.1016/j.neuron.2019.06.016.
16. Akiyama, T., Carstens, M.I., Ikoma, A., Cevikbas, F., Steinhoff, M., and Carstens, E. (2012). Mouse model of touch-evoked itch (alloknesis). J. Investig. Dermatol. *132*, 1886–1891. https://doi.org/10.1038/jid.2012.52.
17. Hill, R.Z., Loud, M.C., Dubin, A.E., Peet, B., and Patapoutian, A. (2022). PIEZO1 transduces mechanical itch in mice. Nature *607*, 104–110. https://doi.org/10.1038/s41586-022-04860-5.
18. Akiyama, T., Nguyen, T., Curtis, E., Nishida, K., Devireddy, J., Delahanty, J., Carstens, M.I., and Carstens, E. (2015). A central role for spinal dorsal horn neurons that express neurokinin-1 receptors in chronic itch. Pain *156*, 1240–1246. https://doi.org/10.1097/j.pain.0000000000000172.
19. Bourane, S., Duan, B., Koch, S.C., Dalet, A., Britz, O., Garcia-Campmany, L., Kim, E., Cheng, L., Ghosh, A., Ma, Q., et al. (2015). Gate control of mechanical itch by a subpopulation of spinal cord interneurons. Science *350*, 550–554. https://doi.org/10.1126/science.aac8653.
20. Feng, J., Luo, J., Yang, P., Du, J., Kim, B.S., and Hu, H. (2018). Piezo2 channel-Merkel cell signaling modulates the conversion of touch to itch. Science *360*, 530–533. https://doi.org/10.1126/science.aar5703.
21. Feng, J., Zhao, Y., Xie, Z., Zang, K., Sviben, S., Hu, X., Fitzpatrick, J.A.J., Wen, L., Liu, Y., Wang, T., et al. (2022). Miswiring of Merkel cell and pruriceptive C fiber drives the itch-scratch cycle. Sci. Transl. Med. *14*, eabn4819. https://doi.org/10.1126/scitranslmed.abn4819.
22. Lee, H., Graham, R.D., Melikyan, D., Smith, B., Mirzakhalili, E., Lempka, S.F., and Duan, B. (2022). Molecular Determinants of Mechanical Itch Sensitization in Chronic Itch. Front. Mol. Neurosci. *15*, 937890. https://doi.org/10.3389/fnmol.2022.937890.
23. Ren, X., Liu, S., Virlogeux, A., Kang, S.J., Brusch, J., Liu, Y., Dymecki, S.M., Han, S., Goulding, M., and Acton, D. (2023). Identification of an essential spinoparabrachial pathway for mechanical itch. Neuron *111*, 1812–1829.e6. https://doi.org/10.1016/j.neuron.2023.03.013.
24. Acton, D., Ren, X., Di Costanzo, S., Dalet, A., Bourane, S., Bertocchi, I., Eva, C., and Goulding, M. (2019). Spinal Neuropeptide Y1 Receptor-Expressing Neurons Form an Essential Excitatory Pathway for Mechanical Itch. Cell Rep. *28*, 625–639.e6. https://doi.org/10.1016/j.celrep.2019.06.033.
25. Chen, S., Gao, X.F., Zhou, Y., Liu, B.L., Liu, X.Y., Zhang, Y., Barry, D.M., Liu, K., Jiao, Y., Bardoni, R., et al. (2020). A spinal neural circuitry for converting touch to itch sensation. Nat. Commun. *11*, 5074. https://doi.org/10.1038/s41467-020-18895-7.
26. Fukuoka, M., Miyachi, Y., and Ikoma, A. (2013). Mechanically evoked itch in humans. Pain *154*, 897–904. https://doi.org/10.1016/j.pain.2013.02.021.
27. Reich, A., Mędrek, K., Adamski, Z., and Szepietowski, J.C. (2013). Itchy hair–trichoknesis: a variant of trichodynia or a new entity? Acta Derm. Venerol. *93*, 591. https://doi.org/10.2340/00015555-1543.
28. Rattanakaemakorn, P., and Suchonwanit, P. (2019). Scalp Pruritus: Review of the Pathogenesis, Diagnosis, and Management. BioMed Res. Int. *2019*, 1–11. https://doi.org/10.1155/2019/1268430.
29. Bernhard, J.D. (2017). The itchy scalp. Br. J. Dermatol. *176*, 16–17. https://doi.org/10.1111/bjd.14985.
30. Hurliman, E., Groth, D., Wendelschafer-Crabb, G., Kennedy, W., Kavand, S., Ericson, M., and Hordinsky, M. (2017). Small-fibre neuropathy in a patient with dermatomyositis and severe scalp pruritus. Br. J. Dermatol. *176*, 209–211. https://doi.org/10.1111/bjd.14678.
31. Xu, Z.Z., Kim, Y.H., Bang, S., Zhang, Y., Berta, T., Wang, F., Oh, S.B., and Ji, R.R. (2015). Inhibition of mechanical allodynia in neuropathic pain by TLR5-mediated A-fiber blockade. Nat. Med. *21*, 1326–1331. https://doi.org/10.1038/nm.3978.
32. Jung, W.J., Lee, S.Y., Choi, S.I., Kim, B.K., Lee, E.J., In, K.H., and Lee, M.G. (2018). Toll-like receptor expression in pulmonary sensory neurons in the bleomycin-induced fibrosis model. PLOS One *13*, e0193117. https://doi.org/10.1371/journal.pone.0193117.
33. Ochoa-Cortes, F., Ramos-Lomas, T., Miranda-Morales, M., Spreadbury, I., Ibeakanma, C., Barajas-Lopez, C., and Vanner, S. (2010). Bacterial cell products signal to mouse colonic nociceptive dorsal root ganglia neurons. Am. J. Physiol., Gastrointest. Liver Physiol. *299*, G723–G732. https://doi.org/10.1152/ajpgi.00494.2009.
34. Abraira, V.E., and Ginty, D.D. (2013). The sensory neurons of touch. Neuron *79*, 618–639. https://doi.org/10.1016/j.neuron.2013.07.051.
35. Qi, L., Iskols, M., Greenberg, R.S., Xiao, J.Y., Handler, A., Liberles, S.D., and Ginty, D.D. (2024). Krause corpuscles are genital vibrotactile sensors for sexual behaviours. Nature *630*, 926–934. https://doi.org/10.1038/s41586-024-07528-4.
36. Duan, B., Cheng, L., Bourane, S., Britz, O., Padilla, C., Garcia-Campmany, L., Krashes, M., Knowlton, W., Velasquez, T., Ren, X., et al. (2014). Identification of spinal circuits transmitting and gating mechanical pain. Cell *159*, 1417–1432. https://doi.org/10.1016/j.cell.2014.11.003.
37. Saloman, J.L., Scheff, N.N., Snyder, L.M., Ross, S.E., Davis, B.M., and Gold, M.S. (2016). Gi-DREADD Expression in Peripheral Nerves Produces Ligand-Dependent Analgesia, as well as Ligand-Independent Functional Changes in Sensory Neurons. J. Neurosci. *36*, 10769–10781. https://doi.org/10.1523/JNEUROSCI.3480-15.2016.
38. Shimada, S.G., and LaMotte, R.H. (2008). Behavioral differentiation between itch and pain in mouse. Pain *139*, 681–687. https://doi.org/10.1016/j.pain.2008.08.002.
39. LaMotte, R.H., Shimada, S.G., and Sikand, P. (2011). Mouse models of acute, chemical itch and pain in humans. Exp. Dermatol. *20*, 778–782. https://doi.org/10.1111/j.1600-0625.2011.01367.x.
40. Zheng, Y., Liu, P., Bai, L., Trimmer, J.S., Bean, B.P., and Ginty, D.D. (2019). Deep Sequencing of Somatosensory Neurons Reveals Molecular Determinants of Intrinsic Physiological Properties. Neuron *103*, 598–616.e7. https://doi.org/10.1016/j.neuron.2019.05.039.
41. Rutlin, M., Ho, C.Y., Abraira, V.E., Cassidy, C., Bai, L., Woodbury, C.J., and Ginty, D.D. (2014). The cellular and molecular basis of direction selectivity of Adelta-LTMRs. Cell *159*, 1640–1651. https://doi.org/10.1016/j.cell.2014.11.038.
42. Dhandapani, R., Arokiaraj, C.M., Taberner, F.J., Pacifico, P., Raja, S., Nocchi, L., Portulano, C., Franciosa, F., Maffei, M., Hussain, A.F., et al. (2018). Control of mechanical pain hypersensitivity in mice through ligand-targeted photoablation of TrkB-positive sensory neurons. Nat. Commun. *9*, 1640. https://doi.org/10.1038/s41467-018-04049-3.

43. Seal, R.P., Wang, X., Guan, Y., Raja, S.N., Woodbury, C.J., Basbaum, A.I., and Edwards, R.H. (2009). Injury-induced mechanical hypersensitivity requires C-low threshold mechanoreceptors. Nature *462*, 651–655. https://doi.org/10.1038/nature08505.

44. Lou, S., Duan, B., Vong, L., Lowell, B.B., and Ma, Q. (2013). Runx1 controls terminal morphology and mechanosensitivity of VGLUT3-expressing C-mechanoreceptors. J. Neurosci. *33*, 870–882. https://doi.org/10.1523/JNEUROSCI.3942-12.2013.

45. Ghitani, N., Barik, A., Szczot, M., Thompson, J.H., Li, C., Le Pichon, C.E., Krashes, M.J., and Chesler, A.T. (2017). Specialized Mechanosensory Nociceptors Mediating Rapid Responses to Hair Pull. Neuron *95*, 944–954.e4. https://doi.org/10.1016/j.neuron.2017.07.024.

46. Davidson, S., Copits, B.A., Zhang, J., Page, G., Ghetti, A., and Gereau, R.W.T. (2014). Human sensory neurons: Membrane properties and sensitization by inflammatory mediators. Pain *155*, 1861–1870. https://doi.org/10.1016/j.pain.2014.06.017.

47. Shiers, S., Klein, R.M., and Price, T.J. (2020). Quantitative differences in neuronal subpopulations between mouse and human dorsal root ganglia demonstrated with RNAscope in situ hybridization. Pain *161*, 2410–2424. https://doi.org/10.1097/j.pain.0000000000001973.

48. Ranade, S.S., Woo, S.H., Dubin, A.E., Moshourab, R.A., Wetzel, C., Petrus, M., Mathur, J., Bégay, V., Coste, B., Mainquist, J., et al. (2014). Piezo2 is the major transducer of mechanical forces for touch sensation in mice. Nature *516*, 121–125. https://doi.org/10.1038/nature13980.

49. Sinclair, R., Jolley, D., Mallari, R., Magee, J., Tosti, A., Piracinni, B.M., Vincenzi, C., Happle, R., Ferrando, J., Grimalt, R., et al. (2003). Morphological approach to hair disorders. J. Investig. Dermatol.: Symp. Proc. *8*, 56–64. https://doi.org/10.1046/j.1523-1747.2003.12172.x.

50. Dean, I., and Siva-Jothy, M.T. (2012). Human fine body hair enhances ectoparasite detection. Biol. Lett. *8*, 358–361. https://doi.org/10.1098/rsbl.2011.0987.

51. Cevikbas, F., and Lerner, E.A. (2020). Physiology and Pathophysiology of Itch. Physiol. Rev. *100*, 945–982. https://doi.org/10.1152/physrev.00017.2019.

52. Dong, X., and Dong, X. (2018). Peripheral and Central Mechanisms of Itch. Neuron *98*, 482–494. https://doi.org/10.1016/j.neuron.2018.03.023.

53. Bautista, D.M., Wilson, S.R., and Hoon, M.A. (2014). Why we scratch an itch: the molecules, cells and circuits of itch. Nat. Neurosci. *17*, 175–182. https://doi.org/10.1038/nn.3619.

54. Sharma, N., Flaherty, K., Lezgiyeva, K., Wagner, D.E., Klein, A.M., and Ginty, D.D. (2020). The emergence of transcriptional identity in somatosensory neurons. Nature *577*, 392–398. https://doi.org/10.1038/s41586-019-1900-1.

55. Usoskin, D., Furlan, A., Islam, S., Abdo, H., Lönnerberg, P., Lou, D., Hjerling-Leffler, J., Haeggström, J., Kharchenko, O., Kharchenko, P.V., et al. (2015). Unbiased classification of sensory neuron types by large-scale single-cell RNA sequencing. Nat. Neurosci. *18*, 145–153. https://doi.org/10.1038/nn.3881.

56. Qi, L., Iskols, M., Shi, D., Reddy, P., Walker, C., Lezgiyeva, K., Voisin, T., Pawlak, M., Kuchroo, V.K., Chiu, I.M., et al. (2024). A mouse DRG genetic toolkit reveals morphological and physiological diversity of somatosensory neuron subtypes. Cell *187*, 1508–1526.e16. https://doi.org/10.1016/j.cell.2024.02.006.

57. Andersen, H.H., Akiyama, T., Nattkemper, L.A., van Laarhoven, A., Elberling, J., Yosipovitch, G., and Arendt-Nielsen, L. (2018). Alloknesis and hyperknesis-mechanisms, assessment methodology, and clinical implications of itch sensitization. Pain *159*, 1185–1197. https://doi.org/10.1097/j.pain.0000000000001220.

58. Feng, J., and Duan, B. (2023). Understanding neural mechanisms of mechanical itch. J. Allergy Clin. Immunol. *152*, 32–35. https://doi.org/10.1016/j.jaci.2023.05.002.

59. Rajendran, P.S., Challis, R.C., Fowlkes, C.C., Hanna, P., Tompkins, J.D., Jordan, M.C., Hiyari, S., Gabris-Weber, B.A., Greenbaum, A., Chan, K.Y., et al. (2019). Identification of peripheral neural circuits that regulate heart rate using optogenetic and viral vector strategies. Nat. Commun. *10*, 1944. https://doi.org/10.1038/s41467-019-09770-1.

60. Chen, T.W., Wardill, T.J., Sun, Y., Pulver, S.R., Renninger, S.L., Baohan, A., Schreiter, E.R., Kerr, R.A., Orger, M.B., Jayaraman, V., et al. (2013). Ultrasensitive fluorescent proteins for imaging neuronal activity. Nature *499*, 295–300. https://doi.org/10.1038/nature12354.

61. Agarwal, N., Offermanns, S., and Kuner, R. (2004). Conditional gene deletion in primary nociceptive neurons of trigeminal ganglia and dorsal root ganglia. Genesis *38*, 122–129. https://doi.org/10.1002/gene.20010.

62. Ronan, E.A., Gandhi, A.R., Uchima Koecklin, K.H., Hu, Y., Wan, S., Constantinescu, B.S.C., Guenther, M.E., Nagel, M., Liu, L.Y., Jha, A., et al. (2025). Intradental mechano-nociceptors serve as sentinels that prevent tooth damage. Cell Rep. *44*, 116017. https://doi.org/10.1016/j.celrep.2025.116017.

63. Wang, F., Bélanger, E., Côté, S.L., Desrosiers, P., Prescott, S.A., Côté, D.C., and De Koninck, Y. (2018). Sensory Afferents Use Different Coding Strategies for Heat and Cold. Cell Rep. *23*, 2001–2013. https://doi.org/10.1016/j.celrep.2018.04.065.

64. Cai, W., Zhang, W., Zheng, Q., Hor, C.C., Pan, T., Fatima, M., Dong, X., Duan, B., and Xu, X.Z.S. (2024). The kainate receptor GluK2 mediates cold sensing in mice. Nat. Neurosci. *27*, 679–688. https://doi.org/10.1038/s41593-024-01585-8.

65. Chaplan, S.R., Bach, F.W., Pogrel, J.W., Chung, J.M., and Yaksh, T.L. (1994). Quantitative assessment of tactile allodynia in the rat paw. J. Neurosci. Methods *53*, 55–63. https://doi.org/10.1016/0165-0270(94)90144-9.

Please cite this article in press as: Fatima et al., A specialized population of hair afferents dedicated to transmitting mechanical itch, Neuron (2026), https://doi.org/10.1016/j.neuron.2026.05.017

STAR★METHODS

KEY RESOURCES TABLE

REAGENT or RESOURCE	SOURCE	IDENTIFIER
Antibodies		
Rabbit anti-GFP	Amsbio	Cat# TP401; RRID: AB_10890443
Chicken anti-NF200	Abcam	Cat# ab4680; RRID: AB_304560
Rabbit anti-TH	MilliporeSigma	Cat# AB152; RRID: AB_390204
Rabbit anti-α-CGRP	Peninsula Lab	Cat# T-4032; RRID: AB_518147
Living Colors rabbit anti-DsRed	Takara	Cat# 632496; RRID: AB_10013483
Alexa Fluor 488-conjugated Isolectin GS-IB4	ThermoFisher	Cat# I21411; RRID not available
Goat anti-Rabbit IgG (H+L) Alexa Fluor plus 647	ThermoFisher	Cat# A32733; RRID: AB_2536183
Goat anti-Rabbit IgG (H+L) Alexa Fluor plus 555	ThermoFisher	Cat# A32732; RRID: AB_2633281
Goat anti-Rabbit IgG (H+L) Alexa Fluor plus 488	ThermoFisher	Cat# A32731; RRID: AB_2633280
Goat anti-chicken IgY (IgG) (H+L) Alexa 647	Jackson ImmunoResearch	Cat# 103-605-115; RRID: AB_2337392
Oligonucleotides		
In situ probe-mmu *Tlr5*	Advanced Cell Diagnostics	Cat# 451601
In situ probe-mmu *Calb1*	Advanced Cell Diagnostics	Cat# 428431
In situ probe-mmu *Ntrk2*	Advanced Cell Diagnostics	Cat# 423611
In situ probe-mmu *Piezo2*	Advanced Cell Diagnostics	Cat# 400191
RNAscope Multiplex Fluorescent Reagent Kit v2 Assay	Advanced Cell Diagnostics	Cat# 323100
Hybridization Chain Reaction (HCR) v3 kit	Molecular Instruments	N/A
Calb1-B1 probe (HCR)	Molecular Instruments	NM_009788
Bacterial and virus strains		
AAV-PHP.eB-CAG-DIO-ChR2(H134R)-eYFP	Rajendran et al. (2019)[59]	Cat#: 127090; RRID: Addgene_127090
AAV-PHP.S-FLEX-tdTomato	Edward Boyden via Addgene	Cat#: 28306 RRID: Addgene_28306
AAV9.CAG.Flex.GCaMP6s.WPRE.SV40	Chen et al. (2013)[60]	Cat#: 100842; RRID: Addgene_100842
AAV9.CAG.FLEX-GCaMP7f	Biohippo	Cat# PT-1422
Chemicals, peptides, and recombinant proteins		
Diphtheria toxin	MilliporeSigma	Cat# D0564
Clozapine N-oxide	MilliporeSigma	Cat# C0832
Compound 48/80	MilliporeSigma	Cat# C2313
Chloroquine	MilliporeSigma	Cat# C6628
Me-5-HT	MilliporeSigma	Cat# SML0640
Calcipotriol	Tocris Bioscience	Cat# 2700
Complete Freund's adjuvant	MilliporeSigma	Cat# 344289
Benzyl Alcohol	MilliporeSigma	Cat# 402834
Benzyl Benzoate	MilliporeSigma	Cat# B6630
Fluoro-Gold	Fluorochrome, LLC	Cat# Fluoro-Gold
NeuroTrace™ 435/455	ThermoFisher	Cat# N21479
Tetrodotoxin	Tocris Bioscience	Cat# 1078
NBQX	Tocris Bioscience	Cat# 0373
Experimental models: Organisms/strains		
Mouse: *Advillin*$^{P2A\text{-}Flpo}$	This paper	N/A
Mouse: *Tlr5*$^{P2A\text{-}iCre\text{-}T2A\text{-}EGFP}$	This paper	N/A
Mouse: *Calb1*$^{P2A\text{-}Flpo}$	This paper	N/A
Mouse: *Calb1*^{Cre}	The Jackson Laboratory	RRID: IMSR_JAX:028532

(*Continued on next page*)

Please cite this article in press as: Fatima et al., A specialized population of hair afferents dedicated to transmitting mechanical itch, Neuron (2026), https://doi.org/10.1016/j.neuron.2026.05.017

Continued

REAGENT or RESOURCE	SOURCE	IDENTIFIER
Mouse: *Ntrk2*$^{Cre/ERT2}$	The Jackson Laboratory	RRID: IMSR_JAX:027214
Mouse: *Slc17a8*^{Cre}	The Jackson Laboratory	RRID: IMSR_JAX:018147
Mouse: *Scn10a*^{Cre}	Agarwal et al.[61]	Generated by Kuner Lab
Mouse: *Ucn3*^{EGFP}	MMRRC	RRID: MMRRC_029604-UCD
Mouse: *Piezo2*$^{flox/flox}$	The Jackson Laboratory	RRID: IMSR_JAX:027720
Mouse:*Tau*$^{LSL\text{-}FSF\text{-}DTR}$; (*Tau*$^{ds\text{-}DTR}$)	Duan et al.[36]	Generated by Goulding Lab
Mouse: *Rosa26*$^{LSL\text{-}GCaMP6s}$	The Jackson Laboratory	RRID: IMSR_JAX:024106
Mouse: *Rosa26*$^{LSL\text{-}tdTomato}$	The Jackson Laboratory	RRID: IMSR_JAX:007914
Mouse: *Rosa26*$^{LSL\text{-}FSF\text{-}tdTomato}$; (*Rosa26*$^{ds\text{-}tdTomato}$)	The Jackson Laboratory	RRID: IMSR_JAX:021875
Mouse: *Rosa26*$^{LSL\text{-}FSF\text{-}ReaChR\text{-}mCitrine}$; (*Rosa26*$^{ds\text{-}ReaChR}$)	The Jackson Laboratory	RRID: IMSR_JAX:024846
Mouse: *Rosa26*$^{LSL\text{-}FSF\text{-}hM4Di}$; (*Rosa26*$^{ds\text{-}hM4Di}$)	The Jackson Laboratory	RRID: IMSR_JAX:029040
Mouse: *Rosa26* $^{FSF\text{-}eGFP}$	Duan et al.[36]	Generated by Dymecki Lab
Software and algorithms		
Prism10	GraphPad	graphpad.com; RRID: SCR_002798
MetaFluor	Molecular Devices	moleculardevices.com; RRID: SCR_014294
pClamp 10.0	Molecular Devices	moleculardevices.com; RRID: SCR_011323
ImageJ	NIH	imagej.nih.gov/ij; RRID: SCR_003070
MATLAB	MathWorks	mathworks.com; RRID: SCR_001622
Other		
In vivo confocal Ca^{2+} imaging analysis	Ronan et al.[62]	10.1016/j.celrep.2025.116017

EXPERIMENTAL MODEL AND STUDY PARTICIPANT DETAILS

Mice

All animal procedures were conducted in accordance with institutional and national guidelines. Experiments performed at the University of Michigan complied with protocols approved by the Institutional Animal Care and Use Committee and followed NIH guidelines. Experiments performed at Université Laval (Yves De Koninck laboratory) were conducted in accordance with the guidelines of the Canadian Council on Animal Care and were approved by Université Laval's Animal Protection Committee. Both male and female mice were included in all experiments. The mice were housed under standard laboratory conditions, maintained at room temperature, and provided with ad libitum access to standard lab mouse pellet food and water. The mice were kept on a 12-hour light/12-hour dark cycle. Mice used in this study were on a pure 129 or mixed 129-C57BL/6J background. Unless otherwise indicated, mice were 6-12 weeks of age at the time of experimentation.

METHOD DETAILS

Animal generation and handling

Two knock-in mouse lines *Advillin*$^{P2A\text{-}Flpo}$ and *Tlr5*$^{P2A\text{-}iCre\text{-}T2A\text{-}EGFP}$ were generated in this work using the CRISPR/Cas9 technique by the transgenic core at the University of Michigan. Fertilized eggs from mixed C57BL/6J and SJL female mice were microinjected with double-stranded purified DNA. The F1 founders were received and then subsequently validated through long-range PCR and DNA sequencing. The knock-in mouse line *Calb1*$^{P2A\text{-}Flpo}$ was generated in collaboration with Cyagen. The F1 founders were validated through long-range PCR and DNA sequencing by Cyagen. To establish stable lines, these founders were backcrossed to the 129 background for more than six generations.

Neuronal ablation

We ablated DTR-expressing sensory neurons as previously described.[15,36] 6-10 week-old control and ablated mice were administered diphtheria toxin (DT, 25 μg/kg; MilliporeSigma, Burlington, MA) through the intraperitoneal route for five consecutive days. The animals were tested for behavioral paradigms or histochemical experiments 4-6 weeks after DT injection.

Neuronal silencing

For chemogenetic silencing, hM4Di was expressed in targeted neuronal populations. Clozapine-N-oxide (CNO, 5 mg/kg; MilliporeSigma, Burlington, MA) was administered intraperitoneally 30 minutes before behavioral or electrophysiological experiments to transiently silence hM4Di-expressing neurons. Control animals received equivalent injections of vehicle solution.

Please cite this article in press as: Fatima et al., A specialized population of hair afferents dedicated to transmitting mechanical itch, Neuron (2026), https://doi.org/10.1016/j.neuron.2026.05.017

In situ hybridization

Mice were perfused intracardially using 4% paraformaldehyde. DRGs were dissected and fixed in 4% paraformaldehyde (PFA, MilliporeSigma, Burlington, MA) for 2 hours, followed by overnight immersion in 20% sucrose solution, and then embedded in Optimal Cutting Temperature Compound (OCT, Sakura Finetek, Torrance, CA) and snap-frozen for further processing. DRG tissue was equilibrated to -20 °C in a cryostat (Leica, Germany), and serial sections of DRGs were collected at 12 μm. Single-molecule fluorescence *in situ* hybridization was performed using RNAscope Multiplex Fluorescent Reagent Kit V2 (Advanced Cell Diagnostics, Newark, CA; Cat# 323100), and the protocol was followed according to the instructions for fresh-frozen tissue. RNA transcripts were detected by *in situ* hybridization. Detection probes were used from Advanced Cell Diagnostics (Newark, CA) for mouse *Tlr5* (C1; 451601), *Calb1* (C3; 428431-C3), *Ntrk2* (C2; 423611-C2), *Piezo2*-E43-E45 (C2; 400191-C2). Briefly, tissue sections were fixed with 4% PFA in phosphate-buffered saline (PBS) for 15 min at 4 °C and pretreated with protease IV for 30 min. Sections were incubated with commercially available or custom-designed probes. Probes were fluorescently labeled with orange (excitation 570 nm), green (excitation 520 nm), or far-red (excitation 647 nm) fluorophores. For double staining analyses of tdTomato fluorescence coupled with ISH, the tdTomato fluorescent signal was first imaged under a fluorescent microscope (Leica DMi8, Germany) prior to performing RNAscope. After RNAscope, the pseudo-fluorescent signals were converted from bright field images and then merged onto the tdTomato images using Adobe Photoshop CS (Adobe Systems, San Jose, CA). Around 200-500 neurons from each animal were analyzed for mRNA transcripts. For the categorization of Piezo2 expression in TLR5$^+$ sensory neurons, a size distribution of TLR5$^+$ sensory neurons was generated. Neurons with a surface area < 400 μm^2, 400-600 μm^2, and > 600 μm^2 were categorized as small-diameter, medium-diameter, and large-diameter cells, respectively.

Immunochemistry

Sections of mouse DRG tissue on slides were washed in PBS for 2 minutes, three times, and incubated in blocking buffer (10% Normal Goat Serum with 0.2% Triton X-100 in PBS) for 30 minutes at room temperature. Slides were incubated in primary antibodies overnight at 4 °C in blocking buffer: 1:1000 rabbit anti-GFP (Amsbio, Abingdon, UK; TP401), 1:500 chicken anti-NF200 (Abcam, Cambridge, UK; ab4680), 1:1000 rabbit anti-TH (MilliporeSigma, Burlington, MA; AB152), 1:500 rabbit anti-α-CGRP (Peninsula Laboratories, San Carlos, CA; T-4032), 1:1000 Alexa Fluor 488-conjugated Isolectin GS-IB4 (ThermoFisher, Waltham, MA; I21411). The following day, sections were rinsed 3 × 5 minutes in PBS and incubated in goat anti-rabbit Alexa 647 (ThermoFisher, Waltham, MA; A32733, 1:1000), anti-rabbit Alexa 555 (ThermoFisher, Waltham, MA; A32732, 1:1000), goat anti-rabbit Alexa 488 (ThermoFisher, Waltham, MA; A32731, 1:1000), and goat anti-chicken Alexa 647 (Jackson ImmunoResearch Laboratories, West Grove, PA; 103-605-115, 1:1000) for 1 hour at room temperature. Slices were washed 3 × 10 min with PBS, incubated in DAPI at 1:5000, and mounted using Fluoromount™ Aqueous Mounting Medium (ThermoFisher, Waltham, MA; F4680).

Cell counting

For neurochemical analysis, cervical DRGs were analyzed from 3-5 mice. Each DRG was sectioned at a thickness of 12 μm, and adjacent sections were distributed over 6 slides. For counting, one of the six slides was used for further processing. Cells showing nuclei were counted. Represented cell counts are cumulated pools of neurons from 6-8 different DRGs, which were from 3-5 different animals. For testing ablation efficiency, the lumbar DRG was tested and quantified for tdTomato signals overlapped with NeuroTrace Nissl staining (ThermoFisher, Waltham, MA).

Skin staining

After euthanizing the animal, excess connective tissues attached to the skin were removed, and tissue sections were fixed in 4% PFA at 4 °C. After fixation, skin tissues were briefly rinsed with PBS and then washed every 30 minutes at room temperature for 4-5 hours in PBS, followed by an additional 4-5 hours of washing in PBS containing 0.1% or 0.5% Triton X-100 (PBST). Living Colors rabbit anti-DsRed (Takara, Mountain View, CA; #632496, 1:500) was diluted in blocking solution (PBST, 20% DMSO, 10% Normal Donkey Serum), and the tissue was incubated in primary cocktail on rocking platform at room temperature for 3-4 days. The tissue was then washed every 30 min in PBST for 2 hours, and the secondary antibodies, goat anti-rabbit Alexa 647 (ThermoFisher, Waltham, MA; A32733, 1:500) and anti-rabbit Alexa 555 (ThermoFisher, Waltham, MA; A32732, 1:500), were added in blocking solution, and the tissue was incubated in secondary cocktail on rocking platform for 2-3 days at room temperature. The tissue was then washed in 0.5% PBST for 5 hours with buffer changed every hour, and dehydrated in MeOH/PBS gradients (25%, 50%, 75%) for 5 minutes each and incubated in 100% MeOH overnight on a rocking platform at room temperature. The following day, the tissue was cleared in MeOH: BABB (1 part Benzyl Alcohol, 2 parts Benzyl Benzoate) for 2 hours on a rocking platform at room temperature, followed by 5 minutes of incubation in BABB, and the tissue was mounted using BABB. The whole mount tissue was imaged using confocal microscopy (Leica Sp8, Germany).

Subcutaneous Fluoro-Gold (FG) injection

Mice were anesthetized under isoflurane. To label the soma of the innervating DRG neurons, 0.25 μl of 4% retrograde tracer Fluoro-Gold (FG) was injected subcutaneously in 6-8-week-old animals. The FG was injected at 2-3 discrete spots in the skin region around the postauricular area so that most of the special hair-innervating skin zone was covered. The animals were sacrificed after 4-5 days of FG injection to analyze the labeled neurons.

Please cite this article in press as: Fatima et al., A specialized population of hair afferents dedicated to transmitting mechanical itch, Neuron (2026), https://doi.org/10.1016/j.neuron.2026.05.017

In vivo two-photon Ca^{2+} imaging

All experiments were performed in accordance with the regulations of the Canadian Council on Animal Care. *Rosa26*$^{LSL\text{-}GCaMP6s}$ mice were crossed with *Tlr5*^{iCre} mice to make *Tlr5*^{GCaMP6s} mice. In order to label $Na_v1.8^+$ sensory neurons, newborn *SNS*^{Cre} mice[61] at P3 to P7 were injected intraplantarly with 10 μl of AAV9.CAG.Flex.GCaMP6s.WPRE.SV40 (Addgene, Watertown, MA; 100842-AAV9).[60,63]

Adult *Tlr5*^{GCaMP6s} or *SNS*^{GCaMP6s} mice were deeply anesthetized intraperitoneally with 100 mg/kg ketamine, 15 mg/kg xylazine, and 2.5 mg/kg acepromazine (MilliporeSigma, Burlington, MA; A7111). Laminectomy was performed to expose the L4-L5 DRG, while the spinal columns flanking the laminectomy site were clenched with two clamps of a home-made spinal stabilization device to fix the animals. 3% agar solution was used to make a pool for holding Ringer solution (in mM: 126 NaCl, 2.5 KCl, 2 $CaCl_2$, 2 $MgCl_2$, 10 D-Glucose, 10 HEPES, pH = 7.0). Dextran Texas Red (70 kDa, Neutral, D1830; ThermoFisher, Waltham, MA; 1% in saline) was injected intravenously to label the blood vessels, which provided structural landmarks for the image registration. The animal was warmed with a heating pad during the surgery and imaging to keep the body temperature at 37 °C. Warmed Ringer solution was dropped on the exposed spinal cord and DRG to keep it moisturized, and repeatedly changed during the imaging experiment. Animals with the whole spinal stabilization device were fixed under a home-made video-rate two-photon microscope. A tunable InSight X3 femto-second laser (Spectra- Physics, Santa Clara, CA) was set to 940 nm for GCaMP6s and Texas Red imaging. Images were acquired at 32 Hz with an Olympus water-immersion 40x objective at a resolution of 0.375 μm/pixel (Olympus, Japan).[63]

Five, well-separated, innocuous stroking stimuli lasting about 15 s were performed on the lateral side of the hindpaw enriched with Type 3 VLHs using a small painting brush. A dual-mode indenter (Aurora Scientific, Aurora, ON, Canada; 300C-I) was modified to deliver feedback-controlled mechanical indentation stimuli. The probe was equipped with a 2 mm diameter tip to provide innocuous stimulations.

In vivo confocal Ca^{2+} imaging

We used *in vivo* confocal Ca^{2+} imaging to monitor stimulation-evoked activity in large populations of $TLR5^+$ DRG neurons.[64] *Tlr5*^{iCre}, *Tlr5*^{iCre};Ai14 and *Tlr5*^{iCre};*Piezo2*$^{f/f}$ mice received a 10 μl intrathecal injection of AAV9.CAG.Flex.GCaMP7f (Biohippo, Gaithersburg, MD; #PT-1422) at 4 weeks of age.

Mice were anesthetized with ketamine (100 mg/kg) and xylazine (10 mg/kg), followed by a laminectomy from the L3 to L6 region. The vertebral plate was drilled with a dental drill to create a window, and the transverse process was removed to expose the L4-L5 DRG. Mice were placed on a heating pad to maintain body temperature during surgery and imaging. During imaging, mice were placed on the microscope stage set-up with spinal column clamps for stabilization to minimize movement due to breathing, and anesthesia was maintained under 1.5-2% isoflurane. A confocal laser scanning microscope (FV3000; Olympus, Japan) equipped with a 10x, 0.4 NA air objective lens and a piezo objective scanner (P-725.CDD; Physik Instrumente, Germany) was used to image the whole L4 DRG. Excitation/emission wavelengths of 488/500-540 nm were used to illuminate green fluorescence of GCaMP7f. Time series images were acquired at a rate of one frame every 2.5 s with a 512 x 512 pixels area (z-axis with a thickness of 80 μm).

To deliver mechanical stimuli to the hair follicles, areas enriched in VLH (lateral part of the hindpaw) and pelage hair (dorsal part of the hindpaw) follicles were precisely looped with a custom-made looping device for 10 s at a rate of 2 loops every second during recording. During stimulation, visualization of VLH and pelage hair in the respective regions was achieved by using dental magnifying glasses with light. VLH can be identified by its reflective and less opaque features when illuminated with light. With the aid of dental magnifying glasses, stroking can be reliably applied to the shaft of VLH and pelage hair without any contact with the skin.

Image processing and analysis for *in vivo* Ca^{2+} imaging

In vivo *two-photon* Ca^{2+} *imaging*

The recorded images were processed and analyzed as previously reported.[63] Briefly, the RAW image sequences were converted into TIFF format in ImageJ (NIH, Bethesda, MD), and movement was corrected with rigid body translation alignment based on the 2D cross-correlation in MATLAB (MathWorks, Natick, MA). After background subtraction, rectangular ROIs were manually placed in the cytoplasm of visible neurons. The average fluorescence intensity of a given ROI, *Ft*, was measured by averaging pixel values inside the ROI. Ca^{2+} response traces were calculated as, $\Delta F/F0 = (Ft\text{-}F0)/F0$, where F0 is the fluorescence value at baseline, which was measured as the average of the first two seconds of *Ft*. To avoid aberrant amplification due to small F0 values in some neurons (e.g., low basal fluorescence), when it was < 1, F0 in the denominator, but not in the numerator, was set to 1. The resulting Ca^{2+} time series extracted from the image sequences were synchronized with thermal or mechanical stimulus data series. An integrated interface within a custom tool written in Spike2 (CED, UK) was used to automatically detect and measure positive responses. All traces were also visually inspected to ensure no false positives were included, and no false negatives were missed. Peak amplitude was measured for all responses using automated algorithms. For each neuron, each parameter was measured for each of the positive responses obtained over multiple trials for each stimulus and then averaged. Finally, all the data were merged into a single database, and a Microsoft Excel (Microsoft, Redmond, WA) Pivot Table was used to select the proper subsets for subsequent statistical analyses. Representative images were processed from the standard deviation of 4 seconds of acquisition at 32 Hz (128 images) during the corresponding stimulation conditions (baseline, indentation stimuli, and looping stimuli).

In vivo *confocal* Ca^{2+} *imaging*

Time series images were motion corrected by using customized MATLAB scripts and followed by manual drawing of regions of interest (ROIs) on responding neurons using ImageJ/Fiji (NIH, Bethesda, MD).[62] Subsequently, fluorescence dynamics of the ROIs

Please cite this article in press as: Fatima et al., A specialized population of hair afferents dedicated to transmitting mechanical itch, Neuron (2026), https://doi.org/10.1016/j.neuron.2026.05.017

were analyzed by custom MATLAB scripts. F0 was calculated as an average of 5 frames at baseline, and the normalized GCaMP7f fluorescence was calculated as ΔF/F0 for each ROI. For background noise correction, signals of the region surrounding the drawn somatic ROI were subtracted from the response of the somatic ROI.[45] Neurons were considered responders if ΔF/F0 > 10%.

Post hoc HCR staining for whole mount DRG

After *in vivo* Ca^{2+} imaging of the DRG of $TLR5^{Avil}$-tdT mouse, a Z-projection image of the endogenous tdTomato expression was captured in the same field of view as the recording. The DRG were rinsed with 1x PBS and briefly fixed in ice-cold 4% PFA in 1x PBS. Next, the DRG were dissected and adhered to plastic strips (1.0 x 0.3 cm) with the ventral side facing down. The DRG were further fixed in 4% PFA in 1x PBS on ice for 90 min, followed by 3 times of rinsing with 1x PBS. The HCR staining was performed based on a modified protocol of hybridization chain reaction version 3.3 (Molecular Instruments, Los Angeles, CA).[62] Pre-hybridization in HCR hybridization buffer for 30 min at 35 °C, followed by *Calb1* probe hybridization at 35 °C for 72 h. After probe hybridization, DRG were washed in the following sequence: 15 min in wash buffer at 39°C (two rounds), 30 min in 30% formamide in 2x SSC at 39 °C (four rounds), 2x SSC at room temperature, followed by incubation of 30 min in amplification buffer at room temperature. The signals were then amplified by incubating in amplification buffer containing amplifier hairpins for adapters B1 conjugated to AlexaFluor647, prepared as suggested by the manufacturer (Molecular Instruments, Los Angeles, CA). Following amplification, DRG were washed in 5x SSC in 0.1% Tween for 30 min in the dark, then embedded in 2% low-melt agarose. The DRG were immersed in imaging buffer (3 U/mL pyranose oxidase, 0.8% D-glucose, 2x SSC, 10 mM Tris-HCL, RNase inhibitor, pH 7.4) during imaging by using a confocal microscope (Olympus, Japan; FV3000).

For the alignment of *in vivo* Ca^{2+} imaging data with post hoc HCR staining, endogenous tdTomato reference images taken right after *in vivo* Ca^{2+} imaging and post hoc HCR staining were used as guideposts for alignment.[62] To determine the expression of *Calb1* among the responding $TLR5^{+}$ DRG neurons, fluorescence signal for *Calb1* expression was manually identified based on the colocalization with the activated tdTomato-labeled neurons.

Behavioral testing

For the behavioral experiments, littermate animals of both sexes with a 129 genetic background were utilized, except for Piezo2 cKO mice, which had a mixed C57BL/6J x 129 genetic background. The experimenter was blinded to the genotype of the animal. The animals were habituated in the testing apparatus for 30 minutes for 3-5 days. Following habituation, the animals were tested for acute somatosensory behaviors such as rotarod, acute itch, Hargreaves, and pinprick. After the acute behavioral tests, animals were tested for inflammatory pain, neuropathic pain, acute chemical itch, and lastly, the animals were evaluated for chronic itch. For intersectional manipulations, *Cre*- or *Flpo*-negative littermates were used as controls. For Piezo2 cKO mice, $Piezo2^{f/f}$ or $Tlr5^{iCre/+;}Piezo2^{f/+}$ littermates were used as controls.

Vellus-like hair-mediated itch (VLH-itch)

Five days before the experiments, the fur on the nape was shaved off, and VLHs (the pale-yellow hair) around the postauricular area were cut with fine scissors to half or more than half of the original length (~2.5 mm). Mice were habituated for 15 min for 3-5 consecutive days in a behavioral testing apparatus (IITC, Woodland Hills, CA). On the testing day, animals were habituated again for another 15 min. To evaluate VLH-itch, we employed a 4-0 nylon suture fiber loop (Ethicon Inc., Somerville, NJ) attached to a wooden stem (Figure S6A) to deliver looping stimuli to the hair shafts without direct contact with the skin on the postauricular area. Each stimulus set consisted of 1-10 loops applied to VLHs at approximately 0.5 Hz until the animal displayed a scratching response. A positive response, indicated by the hindpaw scratching towards the looping site, was assigned a score of 1. If no response occurred, the stimulus set was terminated after 10 loops, and a score of 0 was assigned. We conducted a total of 10 separate stimulus sets on VLHs in the skin surrounding the postauricular area. Mice received ten separate sets of looping stimuli with 5-second intervals to induce VLH-itch. The cumulative score obtained from the 10 stimulus sets was divided by 10 and expressed as a percentage to represent the VLH-itch score.

Indentation-evoked Itch

As described previously,[15] VLHs in the postauricular region were shaved 5 days prior to behavioral testing. Mice were habituated to the testing environment for 3-5 days and re-habituated for 15 min on the day of testing before assessment. Each mouse received five discrete mechanical stimuli (~1 s duration) delivered at 3-5 s intervals to randomly selected sites on the postauricular skin. Mechanical stimuli were applied to the skin surface using von Frey filaments (North Coast Medical, Gilroy, CA) ranging from 0.08 mN to 10 mN to evoke hindpaw scratching responses.

Acute chemical itch

For evaluating chemical itch, the fur on the nape was shaved off 5 days before the tests, and the animals were habituated in the testing apparatus for 3-5 days and habituated again for another 15 minutes on the day of testing. Compound 48/80 (100 μg; MilliporeSigma, Burlington, MA), chloroquine (200 μg; MilliporeSigma, Burlington, MA), or Me-5-HT (50 μg; MilliporeSigma, Burlington, MA) in 50 μl of sterile saline was injected intradermally into the nape. The animal behavior was recorded and later analyzed. Scratching bouts were counted for 30 min after injection and represented as a scratching score.

Please cite this article in press as: Fatima et al., A specialized population of hair afferents dedicated to transmitting mechanical itch, Neuron (2026), https://doi.org/10.1016/j.neuron.2026.05.017

Rotarod

To evaluate sensory-motor performance, animals were placed on an accelerating rotarod (IITC, Woodland Hills, CA), and the time to fall off the rod was recorded in three different trials. The latency to fall was determined as the average of 3 trials per animal performed at 10-minute intervals.

Hargreaves

Mice were habituated for 15 min for 3-5 consecutive days in a behavioral testing apparatus (IITC, Woodland Hills, CA). Before the actual test, mice were placed in plastic enclosures and habituated again for another 15 min on the testing day. To assess the latency for experiencing thermo-pain, animals were placed in the testing chamber, and the plantar paw surface was exposed to a beam of radiant heat. The latency to withdraw the paw from the heat source was recorded and averaged from three different trials for each animal. Each trial was separated by at least 10 minutes. A cutoff of 30 seconds of radiant exposure was set to prevent tissue damage.

Acute mechanical pain and noxious pain

To test acute mechanical pain or noxious pain, the animals were placed on an elevated grid, and the lateral plantar surface of the hindpaw was stimulated using von Frey filaments (North Coast Medical, Gilroy, CA) with ascending strength (0.008-2 g) for the von Frey assay (acute mechanical pain) or a pin without skin penetration for the pinprick assay (noxious mechanical pain). For acute mechanical pain, responses from three trials within 1 minute for filament strength were recorded to compute a response score. The paw withdrawal threshold was determined using Dixon's up-down method.[65] For the pinprick assay, responses from 10 trials with a 1-minute interval were used to calculate a score.

Acute optogenetic behavior assay

The pelage hairs around the postauricular area or dorsal hindpaw were trimmed 5 days before tests. *Tlr5*^{iCre};*Avil*^{Flpo};*ReaChR* mice or *Calb1*^{Cre} mice with injection of AAV-PHP.eB-CAG-DIO-ChR2(H134R)-eYFP virus (Addgene, Watertown, MA)[59] was used for the experiments. Mice were habituated for 15 min for 3-5 consecutive days in a behavioral testing apparatus (IITC, Woodland Hills, CA). On the testing day, mice were placed in the plastic enclosures and habituated for another 15 min. Mice then received ten separate laser stimuli for ~2 s at 5 s intervals at randomly selected sites on the skin around the postauricular area or dorsolateral surface of the hindpaw. Laser stimuli (473 nm, 10 mW, 10 Hz) were delivered with an optic fiber (Laserglow technologies, ON, Canada) to determine the adequate power and frequency that evoked the light-induced behavior. The number of events for behavior such as scratching, hindpaw biting, wiping, rubbing, or licking toward the stimulating site, was counted. If the animal responded with hindpaw biting followed by licking, it was considered a biting response since the animal seemingly relieved itself by licking the skin area to subdue the pain caused by biting. The percentage of positive responses in 10 stimuli was measured to indicate a response score.

Histamine-induced alloknesis

The fur on the nape of the neck was shaved 5 days before treatment. On testing day, histamine (50 μg; MilliporeSigma, Burlington, MA) in 10 μl saline was injected intradermally in the middle of the nape.[16] 30 min after injection, mice received three separate innocuous mechanical stimuli for ~1 s delivered using a von Frey filament (0.7 mN; North Coast Medical, Gilroy, CA) at 3-5 s intervals at randomly selected sites oriented radially 0.5-1 cm away from the injection site. The scratching response of hindpaw toward the poking site was considered a positive response. The alloknesis score was counted as the positive responses to three stimuli. Mice repeatedly received the test for 30 min at a 5-min interval (30 min-60 min after injection, a total of seven tests). The overall alloknesis score was calculated as the sum of individual alloknesis scores from seven tests.

Hair pulling-induced behavioral assay

To assess behavioral responses evoked by forceful hair stimulation, a hair pulling assay was performed using forceps (Fine Science Tools, Foster City, CA; #11602-14). Mice were habituated to the testing chamber for at least 30 minutes prior to the experiment. For postauricular stimulation, VLHs in the postauricular skin (~10 individual hairs) were gently grasped with the forceps and pulled upward with a brief, controlled force. For nape stimulation, hairs (~10 individual hairs) within the nape region, consisting predominantly of pelage hairs, were similarly grasped and pulled. Each trial consisted of three independent hair-pulling stimuli, delivered with several seconds between pulls. Behavioral responses were scored immediately following each stimulus by an experimenter blinded to genotype. Responses were categorized as positive if mice exhibited head/body shaking, scratching, or rapid movements. The response score for each mouse was calculated as the number of positive responses out of three stimuli and averaged across trials when applicable. All behavioral testing was performed under ambient lighting conditions, and the same experimenter conducted all assays to ensure consistency.

Chronic itch model of atopic dermatitis

VLHs around the postauricular area were trimmed off to half of the original length, and the surrounding hair of the nape was shaved off 5 days before treatment. The skin around the postauricular area of the animal was topically challenged with 2 nmol of calcipotriol (MC903; Tocris Bioscience, UK) dissolved in 20 μl of ethanol for 5 consecutive days on the left ear of the animal. On day 5 of the

Please cite this article in press as: Fatima et al., A specialized population of hair afferents dedicated to transmitting mechanical itch, Neuron (2026), https://doi.org/10.1016/j.neuron.2026.05.017

calcipotriol treatment, mice were habituated for 15 minutes in the behavioral apparatus and then evaluated for VLH-trichoknesis by using a nylon loop to gently loop VLHs in the skin around the postauricular area. Also, indentation sensitization was tested by delivering 0.7 mN mechanical force to the skin area around the postauricular area for 5 times at a time interval of every 3-5 s at random sites in the skin around the postauricular area. Scratching responses to VLH looping or poking were calculated as a percentage to represent the trichoknesis or alloknesis score. After 7-8 consecutive calcipotriol treatments were completed, mice were habituated for 15 minutes in the behavioral apparatus, then spontaneous scratching bouts were measured for 30 minutes.

Spared nerve injury-induced pain

The spared nerve injury (SNI) model was used to evaluate neuropathic pain. Animals were kept under isoflurane during the surgery (inhalation with 5% for induction and 2% for maintenance). The sciatic nerve of the animal was exposed by making an incision in the thigh region of the animal. The tibial and peroneal branches of the sciatic nerve were located and cut while leaving the sural nerve intact. After the surgery, the plantar region innervated by the sural nerve ipsilateral to the surgery side was mechanically poked by an ascending force of von Frey filaments (North Coast Medical, Gilroy, CA) to evaluate mechanical allodynia, and the withdrawal threshold was calculated by Dixon's up-down method.[65]

Inflammatory pain

For CFA-induced inflammatory pain, mice were briefly anesthetized with isoflurane (3-5 min at 2%), and 20 μl of Complete Freund's Adjuvant (CFA; MilliporeSigma, Burlington, MA) was injected into the plantar surface of the left hindpaw. Mechanical allodynia was measured 1 and 3 days after CFA injection using von Frey.

Flagellin-induced scratching and pharmacological silencing

To evoke scratching behavior, flagellin (0.9 μg; MilliporeSigma, Burlington, MA) was dissolved in 20 μl of sterile saline and administered by intradermal injection into the postauricular skin. Scratching responses were monitored immediately after injection for 30 min. For pharmacological silencing of TLR5^{+} Aβ-LTMRs, flagellin (0.9 μg; MilliporeSigma, Burlington, MA) was co-administered with QX-314 (1%; MilliporeSigma, Burlington, MA) dissolved in PBS, with a total injection volume of 20 μl delivered intradermally to the same skin region. Optogenetic activations were performed 90 min after injection. As a control, 20 μl of PBS was injected intradermally into the same region using identical procedures.

Intra-DRG injection of AAV virus

Mice were anesthetized with isoflurane (inhalation with 5% for induction and 2% for maintenance). The surgical site of the mice on the back was shaved and sterilized with an alcohol swab. An incision was made to expose L3 and L4 segments of the spine, which were then fixed on the stereotaxic instrument (David Kopf, Tujunga, CA). Hemi-laminectomy was performed on the unilateral side of mice, and the corresponding L3 and L4 DRGs were exposed. A micro syringe pump with a glass electrode filled with AAV.PHP.eB-CAG-DIO-ChR2(H134R)-eYFP (Addgene, Watertown, MA) or AAV.PHP.S-FLEX-tdTomato (Addgene, Watertown, MA) at a concentration of 2×10^{13} GC/ml, was adjusted at about 45 degrees to the spinal column and inserted into L3 and L4 DRG separately. Two sites at one DRG were injected with a depth of about 0.2-0.3 mm and a flow rate of 30 nl/min. The total volume of the injected virus was 300 nl per DRG. Each injection was maintained for 5 min before withdrawal for efficient diffusion. After the virus injection, the incision was closed with a 5-0 Ethicon suture. As per experimental requirements, behavior or skin analyses were performed after 4 weeks of recovery for maximum virus transfection.

Human DRG culture

Dissociated adult human dorsal root ganglia (hDRGs) from consented donors were obtained as primary mixed cultures containing neurons and glial cells (AnaBios, San Diego, CA). Upon arrival, cell suspensions were washed in DMEM/F12 (ThermoFisher, Waltham, MA; #11320033) supplemented with 1% penicillin/streptomycin (ThermoFisher, Waltham, MA; #15140122) and resuspended to the appropriate density. Cells were plated immediately onto poly-D-Lysine-coated coverslips (Corning Incorporated, Corning, NY; # 354087). After seeding, cells were incubated at 37 °C in a humidified 5% CO_2 incubator for a minimum of 3 hours to allow adhesion. After confirming stable cell adhesion, 1 ml of culture medium was gently added along the wall of the well to avoid disrupting the cells on the coverslip. Culture medium was prepared as follows: DMEM/F12 supplemented with 10% horse serum (ThermoFisher, Waltham, MA; #16050130), 25 ng/ml hNGF (Elabscience, Houston, TX; #PKSH033552), 25 ng/ml hGDNF (Elabscience, Houston, TX; #PKSH032488), Gem21 NeuroPlex (GeminiBio, West Sacramento, CA; #400-160-010), and 1% penicillin/streptomycin (ThermoFisher, Waltham, MA). Cultures were maintained under standard conditions and monitored for glial ensheathment. Half of the culture medium was replaced every 2-3 days until downstream experiments.

In vitro Ca^{2+} imaging

Ca^{2+} imaging was performed on an inverted microscope (Olympus IX73, Japan) under a 60x lens as previously described.[15] Cultured hDRG neurons were incubated with 1 μM Fura-2-acetoxymethyl ester (ThermoFisher, Waltham, MA) for 20 min at 37°C, washed three times, and incubated in standard extracellular solution (10 mM HEPES [pH 7.4], 5 mM KCl, 145 mM NaCl, 1.2 mM $MgCl_2$, 2.5 mM $CaCl_2$, and 10 mM glucose) for 30 min. Images were acquired with a Roper CoolSnap CCD camera (Roper Scientific, Trenton,

Please cite this article in press as: Fatima et al., A specialized population of hair afferents dedicated to transmitting mechanical itch, Neuron (2026), https://doi.org/10.1016/j.neuron.2026.05.017

NJ) and processed with MetaFluor software (Molecular Devices, San Jose, CA). Flagellin (5 nM), capsaicin (1 μM), and KCl (50 mM) were dissolved in standard extracellular solution.

Electrophysiology

Whole-cell current-clamp recording in cultured hDRG neurons

Whole-cell voltage-clamp recordings were performed at room temperature using a MultiClamp 700B amplifier and Digidata 1550B controlled by pClamp 10.0 software (Molecular Devices, San Jose, CA). Cells were recorded in a chamber continuously perfused at 5 ml/min with extracellular solution containing (in mM): 126 NaCl, 3 KCl, 2 $CaCl_2$, 1 $MgCl_2$, 26 $NaHCO_3$, and 10 D-glucose, equilibrated with 95% O_2 and 5% CO_2 (pH 7.3-7.4, 300-305 mOsm). Patch pipettes (3-6 MΩ) were filled with internal solution containing (in mM): 140 KCl, 1 $CaCl_2$, 2 $MgCl_2$, 10 EGTA, 10 D-glucose, and 10 HEPES (pH 7.3, 295-300 mOsm). Resting membrane potential was first measured in current-clamp mode immediately after establishing the whole-cell configuration. Cells were then switched to voltage-clamp mode and held at their measured resting membrane potential. Series resistance was compensated by > 80%, and leak subtraction was performed. Signals were filtered at 2 kHz and digitized at 5 kHz.

Spinal cord slice preparation

As described previously,[15] the parasagittal spinal cord slices attached with the full length of the dorsal root and DRG were collected. *Tlr5^{iCre};Avil^{Flpo};Ucn3^{GFP};Rosa26$^{ds\text{-}ReaChR}$* mice were deeply anesthetized with isoflurane, decapitated and the lumbar spinal cord was rapidly removed and placed in an ice-cold modified artificial cerebrospinal fluid (ACSF) containing (in mM): 80 NaCl, 2.5 KCl, 1.25 NaH_2PO_4, 0.5 $CaCl_2$, 3.5 $MgCl_2$, 25 $NaHCO_3$, 75 sucrose, 1.3 sodium ascorbate and 3.0 sodium pyruvate, with pH at 7.4 and osmolality at 310-320 mOsm, bubbled with 95% O_2 and 5% of CO_2. Spinal cord slices (480 μm) attached with dorsal roots and DRGs were cut sagittally by a vibratome (Leica, Germany; VT1200s). The slice was then incubated for about 1 hour at 33°C in oxygenated (95% O_2 and 5% CO_2) cutting solution, which contains (in mM): 125 NaCl, 2.5 KCl, 2 $CaCl_2$, 1 $MgCl_2$, 1.25 NaH_2PO_4, 26 $NaHCO_3$, 25 D-glucose, 1.3 sodium ascorbate, and 3.0 sodium pyruvate, with pH at 7.2 and osmolality at 310-320 mOsm.

Whole-cell patch clamp recording in spinal cord slices

After slice incubation, spinal cord and DRG slices were transferred to a recording chamber and continuously perfused at 5 ml/min with artificial cerebrospinal fluid (ACSF) containing (in mM): 126 NaCl, 3 KCl, 2 $CaCl_2$, 26 $NaHCO_3$, and 10 D-glucose, equilibrated with 95% O_2 and 5% CO_2 (pH 7.3-7.4). Whole-cell patch-clamp recording experiments were then performed on Ucn3^{GFP} dorsal horn neurons at room temperature. Borosilicate glass pipettes (Sutter Instrument, Novato, CA) with resistance of 3-6 MΩ were then filled with an internal solution that contains (in mM): 130 potassium gluconate, 5 KCl, 4 Na_2ATP, 0.5 NaGTP, 20 HEPES, 0.5 EGTA, pH 7.28 with KOH, and measured osmolality at 300-310 mOsm. Data were acquired by pClamp 10.0 software (Molecular Devices, San Jose, CA) with MultiClamp 700B patch clamp amplifier and Digidata 1550B (Molecular Devices, San Jose, CA). Responses were low-pass filtered online at 2 kHz and digitized at 5 kHz.

Electrical stimulation

Dorsal root fibers were stimulated using a suction electrode (A-M Systems™, Carlsborg, WA; #573040) connected to a stimulus isolator. Evoked excitatory postsynaptic currents (elec-EPSCs) were recorded in voltage-clamp mode at a holding potential of -70 mV, near the reversal potential for inhibitory currents, thereby minimizing IPSCs. Inhibitory postsynaptic currents (elec-IPSCs) were recorded at 0 mV, near the reversal potential for glutamatergic currents, to minimize EPSCs. For high-frequency stimulation protocols, trains of 20 stimuli were delivered to assess synaptic reliability and short-term dynamics.

Optogenetic stimulation

ReaChR-expressing TLR5$^+$ afferent terminals were activated by 473 nm LED illumination (1 ms pulses, 5 mW at the slice surface; pE-300White, CoolLED, UK). Light was delivered through the objective to illuminate the recorded region. Optical stimulation was triggered via a Digidata 1550B digitizer controlled by pClamp 10 software (Molecular Devices, San Jose, CA). Light output was calibrated before each experiment to ensure consistent power delivery. Optogenetically evoked EPSCs (optic-EPSCs) were recorded at -70 mV, and optogenetically evoked IPSCs (optic-IPSCs) were recorded at 0 mV. To assess monosynaptic connectivity, high-frequency optical stimulation (10 and 20 Hz) was applied, and light-evoked APs were detected by current-clamp recordings at the resting membrane potential. Pharmacological validation was performed using tetrodotoxin (TTX, 500 nM; Tocris, UK) to block action potential-dependent synaptic transmission and 2,3-Dioxo-6-nitro-1,2,3,4-tetrahydrobenzo[f]quinoxaline-7-sulfonamide disodium salt (NBQX, 20 μM; Tocris, UK) to block AMPA receptor-mediated currents.

Synaptic latency and jitter analysis

Synaptic latency was measured as the time from stimulus onset (electrical or optical trigger) to the onset of the evoked postsynaptic current (PSC). PSC onset was defined as the first point at which the current deflection exceeded baseline noise and continued in the appropriate direction for at least a short window (e.g., 1-2 ms). For each cell, latencies were measured across repeated trials (typically 10-20 sweeps) under identical stimulation conditions.

Jitter was quantified as the trial-to-trial variability in synaptic latency and was calculated as the standard deviation of the latency values across sweeps for each recorded neuron. For group summaries, jitter values were computed per neuron and then averaged across neurons. Low jitter (sub-millisecond) together with high-fidelity responses during high-frequency stimulation was used as supporting evidence for monosynaptic connectivity.

Please cite this article in press as: Fatima et al., A specialized population of hair afferents dedicated to transmitting mechanical itch, Neuron (2026), https://doi.org/10.1016/j.neuron.2026.05.017

Single Cell RT-PCR

PCR-amplified cDNA libraries were generated from individual recorded mouse DRG neurons or human DRG neurons using the SuperScript™ IV Single Cell cDNA PreAmp Kit (#11752048, ThermoFisher, Waltham, MA). The cDNA quality of each cell was confirmed by PCR for Gapdh or GAPDH. Primers were designed using Primer-BLAST for mouse *Gapdh*, *Tlr5*, and *Calb1*, and human *GAPDH*, *TLR5*, *CALB1*, and *NTRK2*. The primer sequences were as follows:

Gapdh (F)TGAAGGTCGGTGTGAACGAATT, (R)GCTTTCTCCATGGTGGTGAAGA;
Tlr5 (F)ACGAGTTCGTCTGCAACTGT, (R)TGACCGTGCACAGGATGAAA;
Calb1 (F)ACTAGCAGAGTACACAGACCTCA, (R)TGTCAGTTCCAGCTTTCCGT;
GAPDH (F)GTCTCCTCTGACTTCAACAGCG, (R)ACCACCCTGTTGCTGTAGCCAA;
TLR5 (F)CCTTACAGCGAACCTCATCCAC, (R)TCCACTACAGGAGGAGAAGCGA;
CALB1 (F)TTTCCTGCTGCTCTTCCGATGC, (R)GCTCCTCAGTTTCTATGAAGCCA;
NTRK2 (F)ACAGTCAGCTCAAGCCAGACAC, (R)GTCCTGCTCAGGACAGAGGTTA.

1x reaction mix, 2 mM $MgCl_2$, 250 μM each deoxynucleotide for each reaction; 0.25 μM forward primer, 0.25 μM reverse primer and 2.5U SuperScript™ One-Step RT-PCR (ThermoFisher, Waltham, MA; #12594025) were combined with 1 μl template cDNA. PCRs were performed with 35 cycles of 10 minutes denaturation (94 °C), 30 seconds denaturation (94 °C), 30 seconds annealing (55 °C), and 2 minutes extension (72 °C) followed by 10 minutes post-elongation (72 °C). Amplified products were run on 1.5% agarose gels. Certain bands were observed in the control DRG neurons, but no bands were seen in the distilled water controls.

QUANTIFICATION AND STATISTICAL ANALYSIS

Results are expressed as mean ± SEM. Statistical analysis was performed in Prism 10 (GraphPad, San Diego, CA). A threshold of $p < 0.05$ was considered statistically significant. For indentation-evoked itch, a different response to different mechanical forces was analyzed with two-way ANOVA with Šídák's multiple comparisons test. For locomotion coordination, touch, chemical itch, acute pain, and inflammatory pain assessment, data were analyzed using a two-tailed unpaired Student's t-test. For SNI-induced neuropathic pain, different time points were assessed by two-way ANOVA with Bonferroni's multiple comparisons test. No statistical methods were used to predetermine sample sizes, but our sample sizes were comparable to those reported in previous publications.[15,36]

ADDITIONAL RESOURCES

No additional resources are available.